Scanning

Novel Scanning Characterization Approaches for the Accurate Understanding and Successful Treatment of Oral and Maxillofacial Pathologies

Lead Guest Editor: Lavinia C. Ardelean
Guest Editors: Laura-Cristina Rusu, Stefan G. Stanciu, and Juan M. Bueno

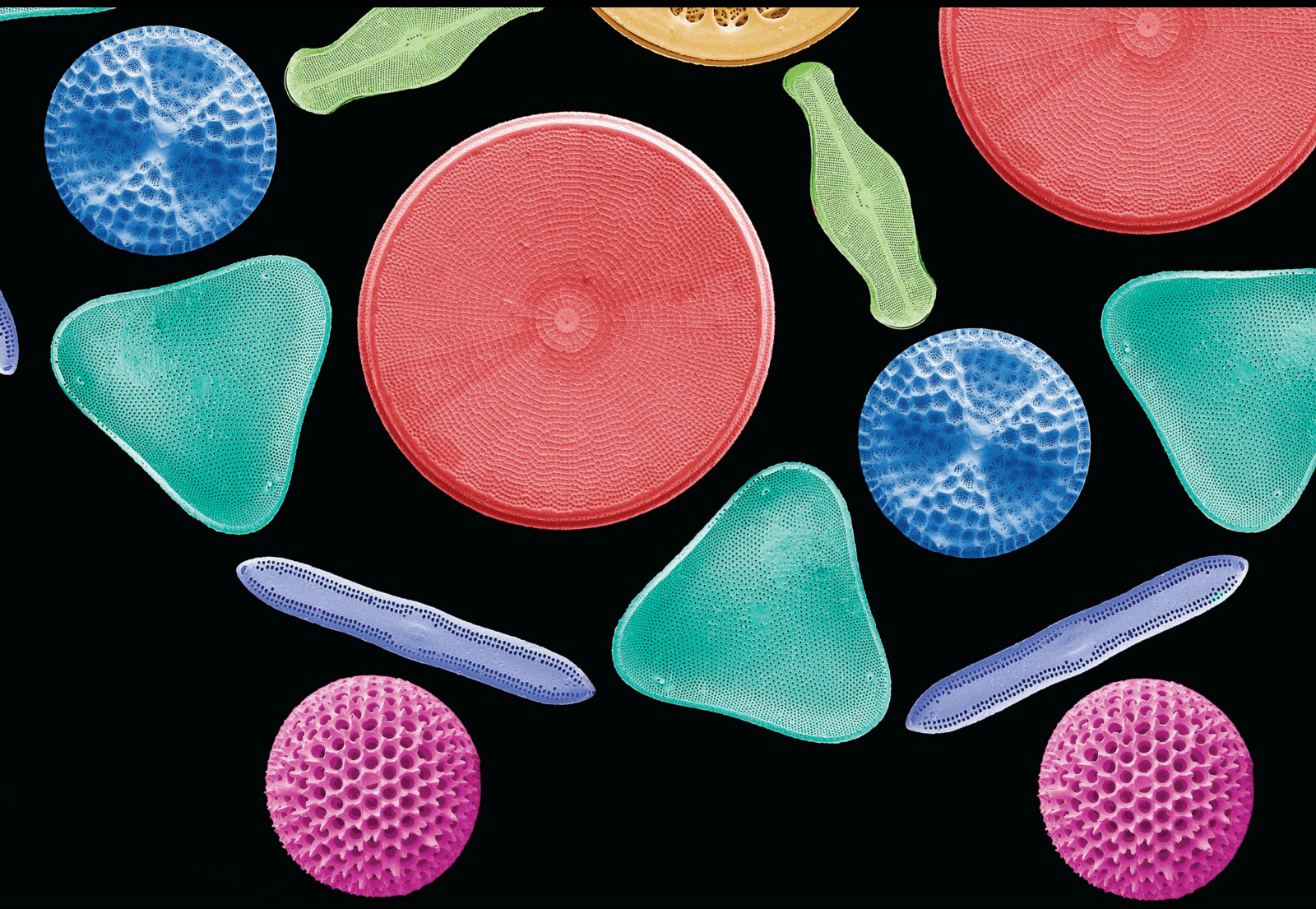

Novel Scanning Characterization Approaches for the Accurate Understanding and Successful Treatment of Oral and Maxillofacial Pathologies

Scanning

Novel Scanning Characterization Approaches for the Accurate Understanding and Successful Treatment of Oral and Maxillofacial Pathologies

Lead Guest Editor: Lavinia C. Ardelean
Guest Editors: Laura-Cristina Rusu, Stefan G. Stanciu, and Juan M. Bueno

Editorial Board

Contents

Hindawi
Scanning
Volume 2020, Article ID 6545823, 2 pages
https://doi.org/10.1155/2020/6545823

Editorial

Novel Scanning Characterization Approaches for the Accurate Understanding and Successful Treatment of Oral and Maxillofacial Pathologies

Lavinia Cosmina Ardelean,[1] **Laura Cristina Rusu**,[2] **Stefan G. Stanciu**,[3] **and Juan M. Bueno**[4]

[1]*Department of Technology of Materials and Devices in Dental Medicine, "Victor Babes" University of Medicine and Pharmacy from Timisoara, Timisoara, Romania*
[2]*Department of Oral Pathology, "Victor Babes" University of Medicine and Pharmacy from Timisoara, Faculty of Dental Medicine, Timisoara, Romania*
[3]*Center for Microscopy-Microanalysis and Information Processing, University Politehnica of Bucharest, Bucharest, Romania*
[4]*Laboratorio de Optica, Universidad de Murcia, Murcia, Spain*

Correspondence should be addressed to Lavinia Cosmina Ardelean; lavinia_ardelean@umft.ro

Received 11 February 2020; Accepted 11 February 2020; Published 19 February 2020

Understanding in detail the modifications that occur in biological tissues during the progression of oral and maxillofacial pathologies requires the use of complementary scanning microscopy techniques. Optical imaging modalities such as multiphoton microscopy (MPM), Coherent Anti-Stokes Raman Scattering Microscopy (CARS), Reflectance Confocal Laser Scanning Microscopy (RCLSM), or optical coherence tomography (OCT) can thus be of great help for improving diagnosis, as they can visualize morphological features and provide information on biochemical modifications specific to various health states. Further on, these techniques can be used in tandem with other complex imaging tools, including Micro-CT, Scanning Electron Microscopy (SEM), or Atomic Force Microscopy (AFM), to shed light over the interactions that take place between soft tissues and advanced materials that are used in various therapeutic approaches, such as micro- and nanostructured polymers, ceramics, and metallic materials. These techniques have applications in diagnostics, theranostics, restorative and regenerative medicine, prosthetics, and other relevant biomedical tasks. Furthermore, to achieve a better understanding of oral and maxillofacial pathologies, these characterization techniques can be coupled with 3D scanning (e.g., intraoral scanning) and 3D printing technologies that are widely used in the dental area, because of their immense benefits. For example, scanning physical models into digital 3D computer-aided (CAD) files to be used in designing and additive manufacturing (CAM) of various prosthetic pieces, and aiding dentists with easier treatment planning, improved communication with laboratories and reduced operative and treatment time. The purpose of this special issue is to present recent progress made in scanning-based tissue imaging, material design and synthesis, and tissue-material interactions, which are relevant with respect to the accurate understanding and successful treatment of oral and maxillofacial pathologies. A brief summary of published papers is provided below.

In the paper of Paul Rotar et al., the accuracy of intraoral scanners used in the dental office, namely, two intraoral scanners Planmeca PlanScan (E4D Technologies, LLC, Richardson, TX, USA) and Omnicam CEREC (Sirona, Bensheim, Germany) as well as a high-resolution desktop scanner, D700, (3Shape, Copenhagen, Denmark), was evaluated. Trueness values were obtained by superimposing the STL files from the test groups with the STL file from the reference scan. Overlapping the STL files within each group generated the precision values. For each set of scans, the mean and standard deviation values were calculated. Statistical analysis was performed using the Kolmogorov-Smirnov

test to assess data distribution. Overall trueness and precision of the scanners were analyzed and compared, and the statistical significance was calculated using the paired *t*-test. The results showed that accuracy deviations of the analyzed scanners were consistent and with no major differences between them.

Michaela Relucenti et al. presented a novel scanning characterization approach, the BSE 3D image analysis, to study the pathological erosion on the surface of human incus bone involved by cholesteatoma, in order to assess the eventual osteoclastic resorptive action. BSE 3D images of resorption pits from osteoporotic human femur neck with that of the incus were compared. Surface parameters were calculated by the software Hitachi Mountains Map© from BSE 3D-reconstructed images; results were then statistically analyzed by SPSS statistical software. The conclusion was that no significant differences exist between the two groups. This quantitative approach implements the morphological characterization, allowing to state that surface erosion of the incus is due to osteoclasts' action. Novel scanning characterization approaches used allowed the 3D imaging of incus bone erosion and its quantitative measurement, opening a new era of quantitative SEM morphology.

Francesco Guido Mangano et al. aimed to present a digital method that combines intraoral and face scanning for the CAD/CAM fabrication of implant-supported bars for maxillary overdentures. 15 patients were rehabilitated with a maxillary overdenture supported by a CAD/CAM polyether-ether-ketone (PEEK) implant-supported bar. The outcomes of the study were the passive fit/adaptation of the bar, the 1-year implant survival, and the success rates of the implant-supported overdentures. The 1-year success rate was of 80% for the implant-supported overdenture leading to the conclusion that the combination of intraoral and face scans allowed to successfully restore fully edentulous patients.

In conclusion, the objectives of the special issue have been reached, several aspects of important interest have been addressed, and the proposed contributions exhibit promising results that outperform existing studies.

Conflicts of Interest

The authors declare that no conflict of interest regarding the publication of this editorial article exist.

Acknowledgments

We would like to express our thanks to all the authors who submitted their articles to this special issue and to all the reviewers who helped us ensure the quality of the papers.

Lavinia Cosmina Ardelean
Laura Cristina Rusu
Stefan G. Stanciu
Juan M. Bueno

Hindawi
Scanning
Volume 2020, Article ID 9371516, 9 pages
https://doi.org/10.1155/2020/9371516

Research Article

SEM BSE 3D Image Analysis of Human Incus Bone Affected by Cholesteatoma Ascribes to Osteoclasts the Bone Erosion and VpSEM dEDX Analysis Reveals New Bone Formation

Michela Relucenti,[1] **Selenia Miglietta**,[1] **Gabriele Bove**,[1] **Orlando Donfrancesco**,[1] **Ezio Battaglione**,[1] **Pietro Familiari**,[2] **Claudio Barbaranelli**,[3] **Edoardo Covelli**,[4] **Maurizio Barbara**,[4] **and Giuseppe Familiari**[1]

[1]*Department SAIMLAL Section of Human Anatomy, Laboratory of Electron Microscopy "Pietro M. Motta", Sapienza University of Rome, Via Alfonso Borelli 50, 00161 Rome, Italy*
[2]*Department NESMOS, Neurosurgery Unit, Sapienza University of Rome, Via di Grottarossa 1039, 00189 Rome, Italy*
[3]*Department of Psychology, Sapienza University of Rome, Via dei Marsi 78, 00185 Rome, Italy*
[4]*Department NESMOS, ENT Unit, Sapienza University of Rome, Via di Grottarossa 1039, 00189 Rome, Italy*

Correspondence should be addressed to Michela Relucenti; michela.relucenti@uniroma1.it

Received 29 July 2019; Accepted 22 January 2020; Published 17 February 2020

Guest Editor: Lavinia C. Ardelean

Bone erosion is considered a typical characteristic of advanced or complicated cholesteatoma (CHO), although it is still a matter of debate if bone erosion is due to osteoclast action, being the specific literature controversial. The purpose of this study was to apply a novel scanning characterization approach, the BSE 3D image analysis, to study the pathological erosion on the surface of human incus bone involved by CHO, in order to definitely assess the eventual osteoclastic resorptive action. To do this, a comparison of BSE 3D image of resorption lacunae (resorption pits) from osteoporotic human femur neck (indubitably of osteoclastic origin) with that of the incus was performed. Surface parameters (area, mean depth, and volume) were calculated by the software Hitachi MountainsMap© from BSE 3D-reconstructed images; results were then statistically analyzed by SPSS statistical software. Our findings showed that no significant differences exist between the two groups. This quantitative approach implements the morphological characterization, allowing us to state that surface erosion of the incus is due to osteoclast action. Moreover, our observation and processing image workflow are the first in the literature showing the presence not only of bone erosion but also of matrix vesicles releasing their content on collagen bundles and self-immuring osteocytes, all markers of new bone formation on incus bone surface. On the basis of recent literature, it has been hypothesized that inflammatory environment induced by CHO may trigger the osteoclast activity, eliciting bone erosion. The observed new bone formation probably takes place at a slower rate in respect to the normal bone turnover, and the process is uncoupled (as recently demonstrated for several inflammatory diseases that promote bone loss) thus resulting in an overall bone loss. Novel scanning characterization approaches used in this study allowed for the first time the 3D imaging of incus bone erosion and its quantitative measurement, opening a new era of quantitative SEM morphology.

1. Introduction

Consensus-based recommendations for the definition of advanced or complicated cholesteatoma (CHO) [1] state that it is an agglomerate of keratinizing squamous epithelium, subepithelial connective tissue, that grows as a progressive accumulation of keratin debris with/without surrounding inflammatory reaction. Regarding its microstructure CHO is made of matrix (keratinized squamous epithelium), perimatrix (subepithelial connective tissue of variable thickness), and keratin debris. Bone erosion is considered a typical characteristic of cholesteatoma; however, it is still a matter of

debate if bone erosion is due to osteoclast action, being present in literature conflicting results [2–7]. Scanning electron microscopy is an elective imaging technique for bone ultrastructural studies [8–12], so we observed by means of innovative SEM BSE 3D imaging and VpSEM EDX analysis that cholesteatoma affected incus bone surface, in order to accurately describe their surface modifications and finally assess if osteoclasts are directly responsible for bone resorption. To accomplish this task, we compared, using SEM BSE 3D imaging analyzed by Hitachi MountainsMap software, the fine structure of resorption pits observed on incus bone surface with the resorption lacunae from osteoporotic femur neck, indubitably of osteoclastic origin. Ultrastructural topography of incus bone surface was also studied through VpSEM EDX analysis.

2. Materials and Methods

2.1. Samples. We observed eighteen incus bones recovered during surgical procedures of CHO removal obtained with patients' informed consent and 1 unaffected incus bone (the control) from cadaver.

We studied eighteen femoral neck biopsies from postmenopausal women with hip arthrosis and osteoporosis who underwent surgical hip substitution, 1 femoral neck biopsy from woman without osteoporosis. BMD and T-score to assess bone osteoporosis condition were evaluated by DEXA (Hologic Delphi) before the surgical operation. Samples were obtained with patients' informed consent.

The study was approved by the Institutional Ethics Board and adhered to the tenets of the Declaration of Helsinki.

2.2. SEM Protocols

2.2.1. Femoral Neck Biopsies. Samples were fixed immediately upon recovery in 2.5% glutaraldehyde in PBS at 4°C for 48 h, then immersed in a 3% hydrogen peroxide solution for 48 h at room temperature (for bone marrow removal), and then rinsed with distilled water. Samples were then sonicated in a sonic device [13] in distilled water at room temperature, rinsed with distilled water, and dehydrated in acetone series. Samples were finally dried using a critical point dryer (Emitech K850, Emitech, Corato, Italy), mounted on aluminum stubs, platinum coated using an Emitech K 550 sputter coater (Emitech, Corato, Italy), and observed by a Hitachi FE SEM S 4000 operating at 7 kV. SEM micrographs were acquired with a DISS5 Digital Image Scanning System (point electronic, Germany).

2.2.2. Incus Preparation Protocol for SEM. Samples were fixed immediately upon recovery in 2.5% glutaraldehyde in PBS at 4°C for 48 h; then, they were gently sonicated in an ultrasonic device (to remove excess of keratinizing squamous epithelium that would have prevented surface observation). Fifteen samples were prepared for SEM (as previously described for femur neck) and sputter coated with platinum using an Emitech K 550 sputter coater (Emitech, Corato, Italy). Observations were conducted by a Hitachi FE SEM S 4000 operating at 7 kV and by a Hitachi SU 3500 (Hitachi High-Technologies Europe GmbH, Mannheim, Germany), at 10 kV in SE mode.

2.2.3. Incus Preparation Protocol for VpSEM and EDX Microanalysis. Three samples, after fixation in 2.5% glutaraldehyde in PBS at 4°C for 48 h, were only gently sonicated in a sonic device [13] and then directly observed by a Hitachi SU 3500 (Hitachi High-Technologies Europe GmbH, Mannheim, Germany), operating at 5 kV and 60 Pa, in BSE COMPO mode without metal coating.

2.3. BSE 3D Image Analysis. Hitachi SU 3500 is equipped with a four-quadrant BSE detector that allows to acquire four images simultaneously with only one scan. The four pictures are then integrated into 3D images and processed to extract quantitative information (all those steps were performed by the software Hitachi Map 3D 7.4 Digital surf, Besançon, France). To obtain this kind of data is extremely useful to implement the morphological classification parameters usually used to characterize resorbing and forming bone surfaces. In fact, acquisition of quantitative resorption pit information such as area, mean depth, and volume allows to compare pits from different sources (femur and incus) and finally assess if they have the same origin. Regions containing resorption bay were analyzed in both incus bone and femur neck samples. BSE 3D images of well delimited resorption pits were acquired, 4 images were combined by the software, and 3D reconstruction was obtained. Resorption pit area, mean depth, and volume were extracted by MountainsMap software after 3D image reconstruction. In more detail, we performed single pit selection on the 3D image reconstruction, followed by automatic measurement of area, mean depth, and volume. Data were collected and statistically analyzed by SPSS statistical software. The following test was performed: summary statistic to assess the normality of distribution of pit area, mean depth, and volume values; independent sample t-test (assuming unequal and equal variances) was used to compare pits area, mean depth, and volume values between incus and femur samples.

2.4. EDX Microanalysis. The variable pressure scanning electron microscopy used in this study (VP-SEM, Hitachi SU3500) is equipped with dual energy dispersive X-ray spectroscopy (dEDS, Bruker XFlash® 6|60) detectors. This instrument has the ability to perform simultaneously multimodal imaging and spatial distribution chemical mapping, a truly powerful analytical approach to study biological surfaces in their native state. The XFlash® 6|60 is particularly suitable for applications with relatively low X-ray yield, as common in the area of nanoanalysis.

2.5. Morphological Classification Parameters for Bone Surface Evaluation. Incus bone areas were classified as resorptive and forming bone surfaces, according to widely accepted morphological criteria described in literature [8–12, 14–17]. Briefly, resorbing bone surfaces are characterized by the presence of large resorption bay or scattered resorption pits (Howship's lacunae). Those structures observed by SEM show shining bright rounded edges, a floor made of partially demineralized collagen bundles and punctuated by

narrow gutters, that appear darker at BSE imaging mode. Bone forming surfaces are characterized by an irregular surface, with collagen bundles undergoing mineralization, mineralizing matrix vesicles and shallow pits (the osteocytic lacunae) in which osteoblast/osteocyte immure themselves. They have an irregular ellipsoidal shape with a large range of variation [18].

3. Results and Discussion

Each CHO incus sample was observed by SEM at low magnification following a precise scanning pathway, in order to assess the general bone morphology and define areas suitable for high magnification observations. This method allowed counting of nutrient foramina opening onto the surface (49 foramina on 18 bones) and identification of areas with marked bone erosion and, interestingly, areas with new bone formation. It is still a matter of debate if bone erosion is due to osteoclast action; moreover, new bone formation was never been described in the incus bone affected by CHO. To get an insight on these findings, we performed observations at magnifications ranging from 400x to 600x, 3D image reconstruction, and EDS analysis.

3.1. Observations of Normal Sample Surface. Before showing images of samples with resorption areas, two images of normal surfaces are presented (Figure 1): normal incus bone surface (Figure 1(a)) and normal trabecular bone (Figure 1(b)). The surface of both bones is devoid of resorption bays.

3.2. Observations of Resorbing Areas. Images of CHO incus bone surface showed 67% of nutritive foramina surrounded by large resorption bays that seem to radiate from nutritive foramen opening (Figures 2(a) and 2(b)).

Observed at higher magnification CHO incus bone resorption bays and pits (Figure 3(a)) resemble in all respects those on the surface of femur neck with osteoporosis (Figure 3(b)).

To definitely assess if incus bone resorption bay is a product of osteoclasts action, we used Hitachi MountainsMap© software to perform a 3D reconstruction from 4 BSE mode images (Figure 4).

A small area was extracted from a 3D-reconstructed image, and each single pit in the small area was analyzed by the software to calculate: area, mean depth, and volume (Figures 5(a) and 5(b)).

We analyzed 79 pits, for each considered parameter values which were recorded and statistically evaluated by SPSS statistical software. Firstly, a summary statistic was performed on data collected for each parameter, to assess normality of distribution (Table 1). For all values, data distribution was normal, so t-test was performed between values of each parameter measured on incus and femur to assess difference between values (Table 2, Figure 6). Two series of independent sample t-test, assuming, respectively, unequal and equal variances, were conducted to compare area, mean depth, and volume values between incus and femur. Both series evidenced that no difference exists between the two groups ($p > 0.05$) for each considered parameter.

3.3. Observation of New Bone-Forming Area. The detailed incus surface observation allowed another interesting finding, the observation of new bone-forming areas on incus surface. Our SEM images are the first to show this process on incus. Mineralizing vesicles releasing their content on collagen bundles are shown in Figures 7(a) and 7(b). SE mode allows the detailed visualization of collagen fibre meshwork while BSE mode clearly points out that matrix vesicles are filled with a high molecular weight content and that collagen bundles have different mineralization degree (lighter or darker areas).

These areas were also analyzed in uncoated samples by variable pressure SEM dEDS analysis. Variable pressure SEM allows the observation of uncoated samples, avoiding metal coating disturbance during elemental analysis. Areas containing calcified matrix vesicles (Figure 8(a)) were analyzed by dEDS. Elemental mapping (Figure 8(b)) clearly shows the presence of calcium in matrix vesicles, while sulphur, contained in matrix proteoglycans, is present only in the surrounding extracellular matrix. Calcium and phosphorus are the characteristic elements of bioapatite [19–21]. The elemental mapping clearly demonstrates that matrix vesicles have a calcium phosphate content.

A later stage in new bone formation is represented by osteocyte self-immuring in forming bone areas. In Figure 9, detailed images of osteocytic lacunae are presented for the first time in which the osteocyte self immure on incus surface. Here again, they are perfectly superimposable with osteocytic lacunae on femur neck samples. Osteocytic lacunae appear surrounded by fully mineralized collagen bundles. At higher magnification (Figure 8(b)), on the floor of the osteocytic lacuna, the not yet fully mineralized collagen fibres and the deep holes are visible in which osteocyte cellular processes nestle.

Prominent theories on bone resorption in CHO are osteoclast activation; pressure necrosis; and acid lysis, enzyme mediation, and inflammatory mediation [22]. The mechanism of bone erosion in middle ear cholesteatoma remains still unclear, although its histopathology has been intensively studied.

In some studies [2, 3], osteoclast was not observed in resorbing bone areas of incus with CHO; in others [4–7], they were reported. This is probably due to the transient nature of osteoclasts; they have a relatively short life and, being surgical procedures done after inflammation control, they may be not present at time of sample recovery and fixation.

Our results showed that no difference exists between area, mean depth, and volume values between incus and femur resorption pit, allowing us to state that surface erosion on the incus is due to osteoclast action.

Osteoclasts are multinucleated cells, they differentiate from monocyte-lineage hematopoietic precursor cells [23]. Macrophage colony-stimulating factor (M-CSF) and receptor activator of nuclear factor κB ligand (RANKL) regulate both differentiation and activation of osteoclasts [24]. In several inflammatory diseases, like rheumatoid arthritis, pathological bone loss is observed, together with RANKL overproduction [25, 26]. Immune cells such as T-lymphocytes and macrophages that infiltrate into damaged areas are major sources of RANKL [27], and fibroblasts in the cholesteatoma

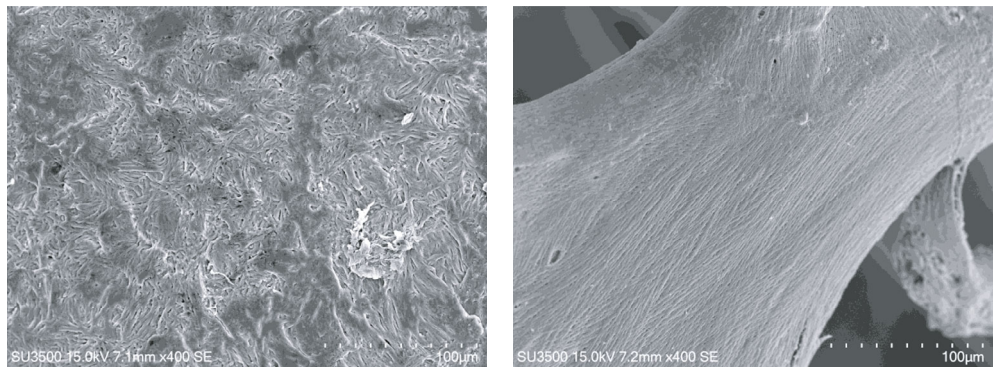

(a) (b)

Figure 1: (a) SE mode, 400x. Incus bone surface from cadaver, normal surface. (b) SE mode, 400x. Trabecular bone from patient without osteoporosis, normal surface.

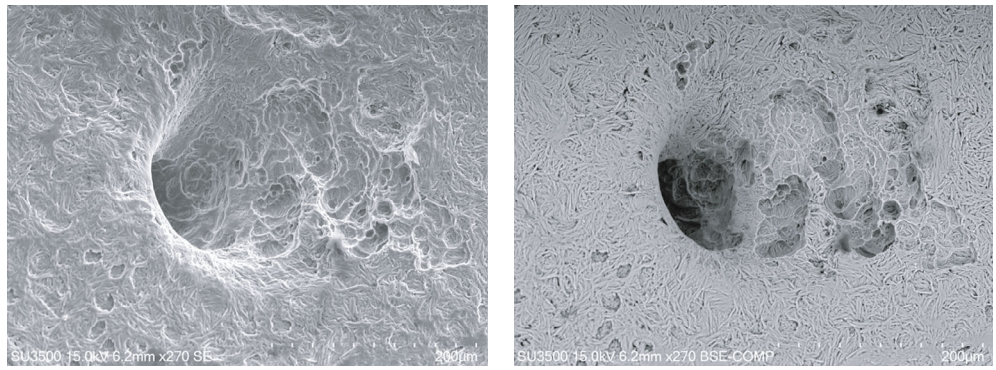

(a) (b)

Figure 2: (a) SE mode, 270x. Nutritive foramen from CHO incus bone. On the right side of the image, large resorption bays, extending since into the foramen, are visible. On the left corner of the picture, osteocytic lacunae are visible. (b) BSE-COMP mode, 270x of same sample. Darker (demineralized) areas correspond to deeper resorption bays. This field shows both bone resorption and bone formation phenomena.

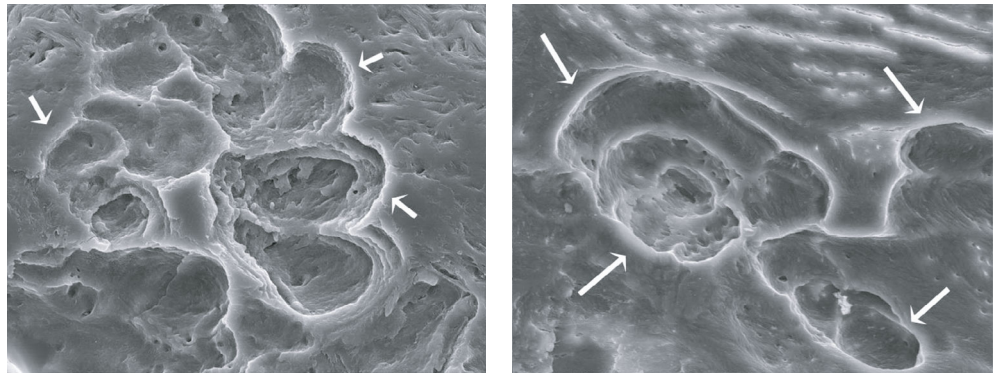

(a) (b)

Figure 3: (a) FE SEM 700x, CHO incus bone resorption bay at higher magnification, osteoclast snake trail pathway is visible (arrows). At the center of the resorption bay, a small promontory rises being relatively resistant to resorption. (b) FE SEM, 600x, osteoclastic resorption bay on osteoporotic human femur neck (arrows), they are unequivocally of osteoclast origin and are undistinguishable from those in (a).

perimatrix express RANKL [28]. The effector cell of focal osteolysis is the osteoclast, but cytokines are key regulators of inflammatory osteolysis [29]. IL-1, IL-6, TNF-α, and prostaglandin E2 (PGE2) have been investigated as inflammatory mediators of cholesteatoma progression. They are assumed to enhance bone resorption by activating osteoclasts [30–32], and inflammation has been confirmed to be essential for cholesteatoma formation, growth, and expansion,

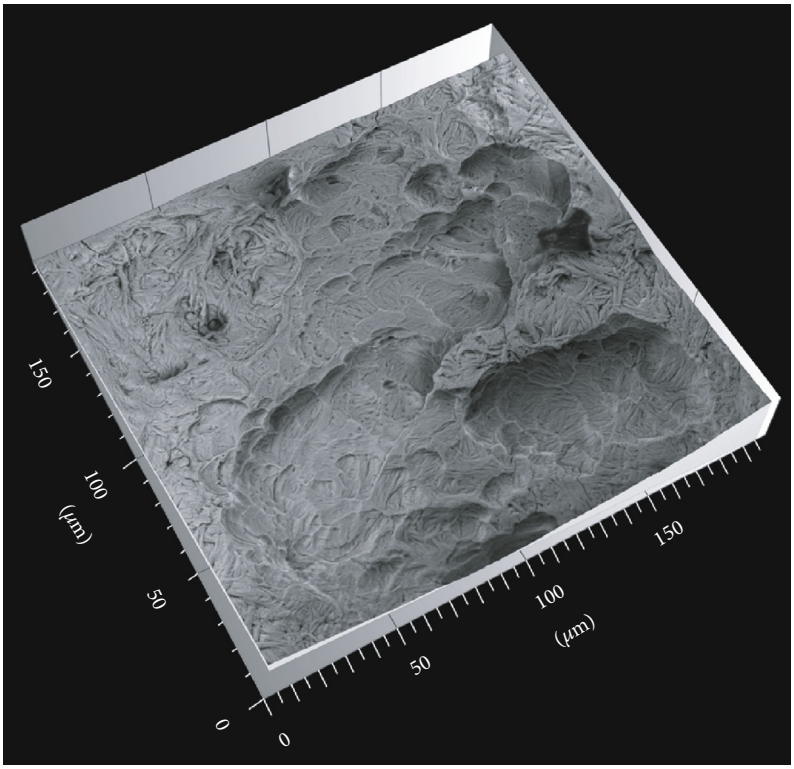

Figure 4: 3D reconstruction from 4 images in BSE mode. Each resorption bay contains several pits.

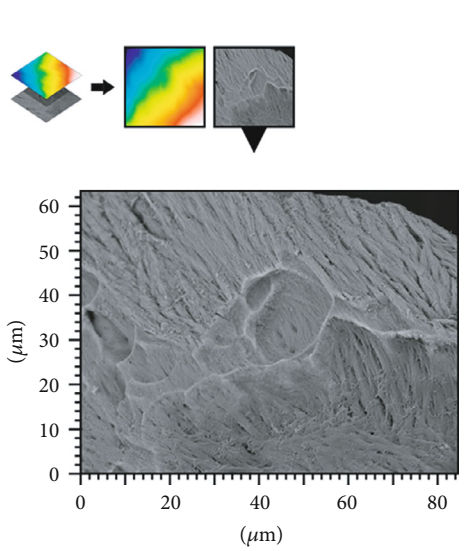

(a)

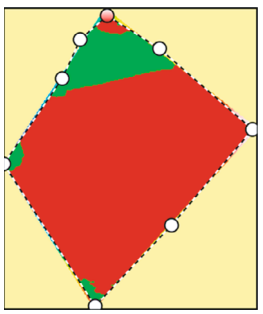

Parameters	Units	Pit	Peak
Area	μm^2	32.4	4.67
Volume	μm^3	14.7	0.459
Max depth	μm	1.15	0.292
Mean depth	μm	0.453	0.0983

(b)

Figure 5: (a) The extracted area of a resorption bay from a larger 3D-reconstructed image. (b) A delimited single pit from which software calculated parameter values.

Table 1: Summary statistic of area, mean depth, and volume values.

Pit	Distribution	Area μm^2 Arithmetic mean ± ds	Mean depth μm Arithmetic mean ± ds	Volume μm^3 Arithmetic mean ± ds
Incus	Normal	120.48 ± 8.54	0.799 ± 0.10	96.48 ± 13.16
Femur neck	Normal	121.34 ± 23.2047	0.784 ± 0.16	94.99 ± 23.65

Table 2: Independent sample t-test on area, mean depth, and volume values.

	Area		Mean depth		Volume	
	Incus	Femur	Incus	Femur	Incus	Femur
Sample size	79	79	79	79	79	79
Arithmetic mean	120.48	121.34	0.799	0.784	96.48	94.99
95% CI for the mean	118.57 to 122.39	116.15 to 126.54	0.77 to 0.82	0.74 to 0.82	93.51 to 99.45	89.69 to 100.28
Variance	72.95	538.45	0.011	0.025	173.31	559.32
St deviation	8.54	23.20	0.10	0.16	13.16	23.65
St error mean	0.96	2.61	0.011	0.018	1.49	2.66
F-test equal variances	$p < 0.001$		$p < 0.001$		$p < 0.001$	
t-test equal variances	$t(156) = 0.310$ $p = 0.7568$		$t(155) = -0.688$ $p = 0.4922$		$t(156) = -0.489$ $p = 0.6258$	
Levene t-test unequal variances	$t(98.76) = 0.310$ $p = 0.7570$		$t(122.43) = -0.688$ $p = 0.4924$		$t(134.18) = -0.489$ $p = 0.6249$	

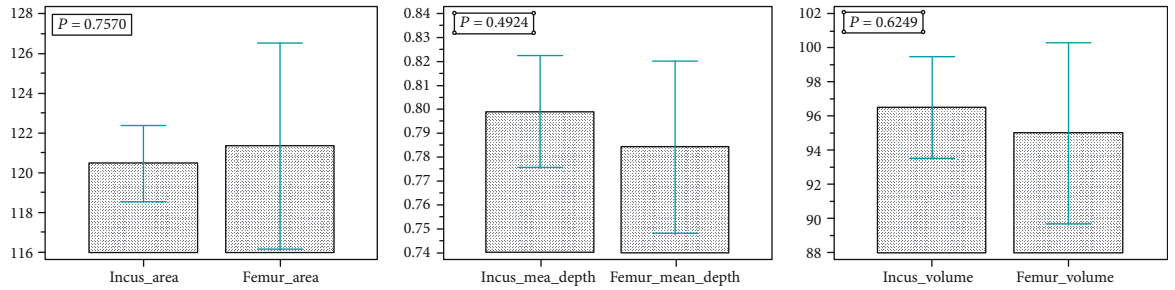

Figure 6: Graphs represent distribution of pit measurement data (from the left to the right): incus area vs. femur area; incus mean depth vs. femur mean depth; incus volume vs. femur volume.

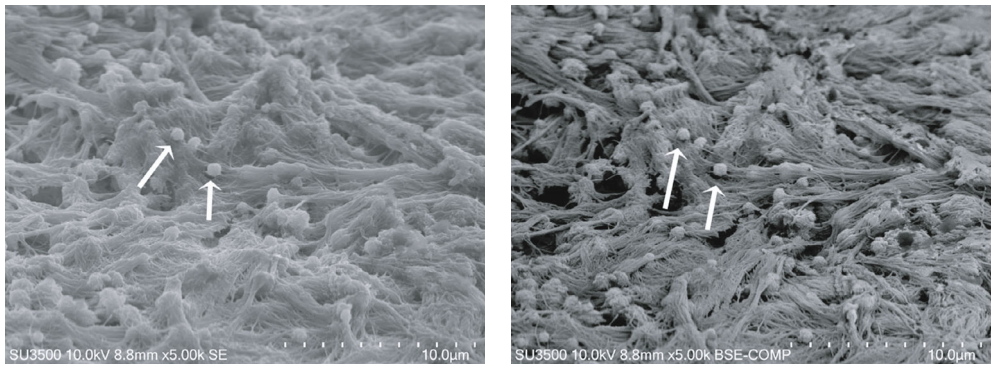

(a) (b)

Figure 7: SE, BSE comp 5000x, new bone formation on CHO incus bone surface. (a) SE mineralizing matrix vesicles releasing their content on collagen bundles (arrows). (b) BSE comp mineralizing matrix vesicles (arrows) appear as bright and rough spheres. Collagen fibres and bundles with variable mineralization degree are visible. Mineralized areas appear lighter at BSE mode.

including the bone resorption process [22, 33, 34]. Inflammatory cells were observed in our samples; in Figure 10, a rare coexistence of a macrophage (blue), a lymphocyte (red), and an osteoclast is presented [35–37].

Bone homeostasis is maintained balancing bone-resorbing osteoclast and bone-forming osteoblast activity, alteration of this balance causes bone loss, that is not recovered by new bone formation. In fact, in inflammation, disease-like RA bone erosion results from excessive bone resorption and markedly limited bone formation [38]. We observed typical morphological markers of new bone formation on incus by CHO, but this phenomenon probably happens at a slower rate than bone resorption, so that bone loss is not compensed.

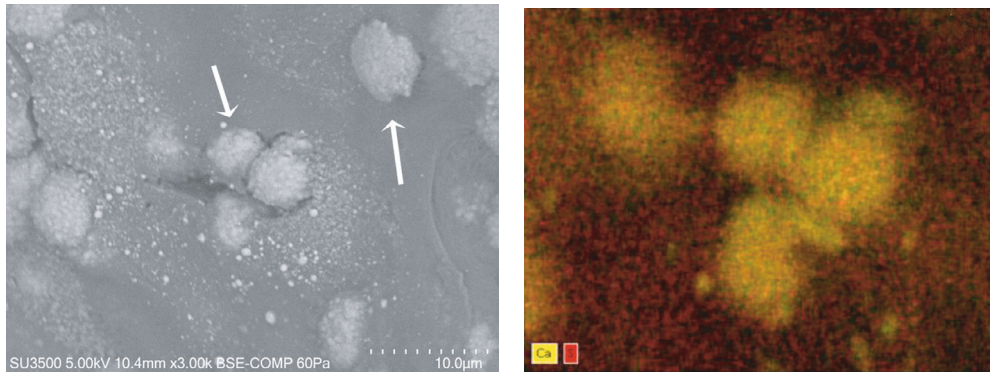

(a) (b)

Figure 8: BSE Comp, 3000x, dEDS analysis, confirmation of new bone formation on CHO incus bone. (a) VP SEM BSE image shows matrix vesicles (arrows). (b) Elemental distribution (dEDS analysis) allows identification of chemical species, calcium in matrix vesicles (yellow) and sulphur in extracellular matrix (red).

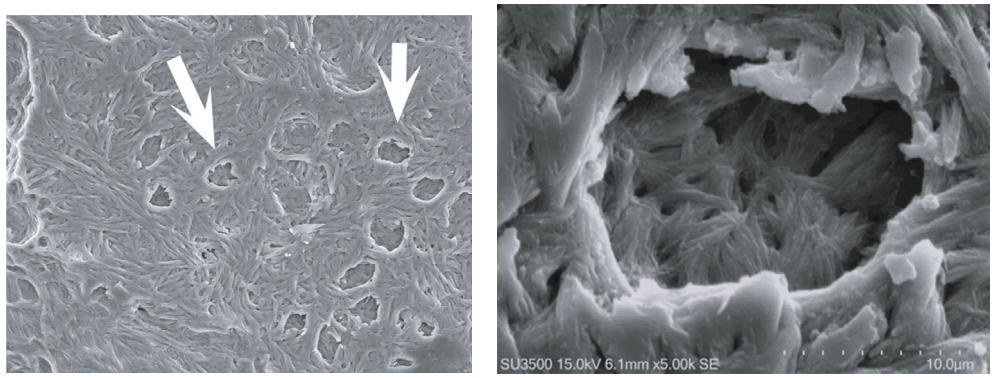

(a) (b)

Figure 9: New bone formation on CHO incus bone surface (a), FE SEM, 250x, osteocytic lacunae (arrows) formed by self-immuring osteocytes. (b) SE, 5000x, high magnification of an osteocytic lacuna, the floor appears less mineralized and spotted by deep holes to accommodate osteocyte cellular processes.

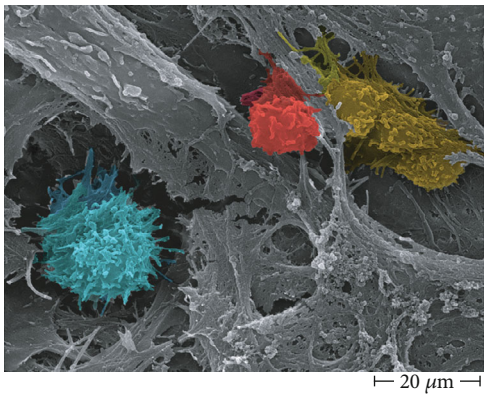

Figure 10: Inflammatory cells and an osteoclast on incus affected by CHO surface, FE SEM 3000x. Active macrophage (blue), lymphocyte (red), and osteoclast (yellow).

4. Conclusions

The innovative quantitative approach used in this paper implements the classical surface morphological characterization, allowing us to state that surface erosion of the incus is due to osteoclast action. Moreover, our observation and processing image workflow are the first in the literature showing the presence not only of bone erosion but also of matrix vesicles releasing their content on collagen bundles and self-immuring osteocytes, all markers of new bone formation on incus bone surface. On the basis of recent literature [22–34], it has been hypothesized that inflammatory environment induced by CHO may trigger the osteoclast activity, eliciting bone erosion; we can provide a morphological evidence of this hypothesis in Figure 9; in fact, a T-lymphocyte, a macrophage, and an osteoclast were photographed one near the other; the photograph gives the impression of witnessing the paracrine molecular dialogue between these cells [22–34]. The observed new bone formation probably takes place at a slower rate in respect to the normal bone turnover, and the process is uncoupled (as recently demonstrated for several inflammatory diseases that promote bone loss) thus resulting in an overall bone loss. Novel scanning characterization approaches used in this study allowed for the first time the 3D imaging of incus bone erosion and its quantitative measurement, opening a new era of biological quantitative

SEM morphology. Taken all together, our morphological results let us hypothesize that cholesteatoma creates an environment of chronic infection with peculiar biochemical characteristics that alters normal bone turnover on incus bone. Targeting the cell population of the inflammatory microenvironment (which produce molecules that stimulate osteoclast activity) will open new therapeutic options, in particular in the field of noninvasive therapies, allowing to inhibit bone erosion development in the acquired middle ear cholesteatoma.

Data Availability

Data are stored in computer of our institution and are available upon request.

Conflicts of Interest

The authors declare that they have no conflicts of interest.

Acknowledgments

This study was funded by the Sapienza University of Rome Research projects funding.

References

[1] E. Olszewska, J. Rutkowska, and N. Özgirgin, "Consensus-based recommendations on the definition and classification of cholesteatoma," *The Journal of International Advanced Otology*, vol. 11, no. 1, pp. 81–87, 2015.

[2] H. Koizumi, H. Suzuki, R. Kawaguchi et al., "Presence of osteoclasts in middle ear cholesteatoma: a study of undecalcified bone sections," *Acta Oto-Laryngologica*, vol. 137, no. 2, pp. 127–130, 2017.

[3] H. Koizumi, H. Suzuki, S. Ikezaki, T. Ohbuchi, K. Hashida, and A. Sakai, "Osteoclasts are not activated in middle ear cholesteatoma," *Journal of Bone and Mineral Metabolism*, vol. 34, no. 2, pp. 193–200, 2016.

[4] R. A. Chole, "Cellular and subcellular events of bone resorption in human and experimental cholesteatoma: the role of osteoclasts," *Laryngoscope*, vol. 94, no. 1, pp. 76–95, 1984.

[5] R. A. Chole, "Osteoclasts in chronic otitis media, cholesteatoma, and otosclerosis," *The Annals of Otology, Rhinology, and Laryngology*, vol. 97, no. 6, pp. 661–666, 1988.

[6] R. Imai, T. Sato, Y. Iwamoto et al., "Osteoclasts modulate bone erosion in cholesteatoma via RANKL signaling," *Journal of the Association for Research in Otolaryngology*, vol. 20, no. 5, pp. 449–459, 2019.

[7] Y. Iwamoto, K. Nishikawa, R. Imai et al., "Intercellular communication between keratinocytes and fibroblasts induces local osteoclast differentiation: a mechanism underlying cholesteatoma-induced bone destruction," *Molecular and Cellular Biology*, vol. 36, no. 11, pp. 1610–1620, 2016.

[8] A. Boyde, "Scanning electron microscopy of bone," in *Bone Research Protocols*, A. I. Idris, Ed., vol. 1914 of Methods in Molecular Biology, Humana Press, New York, NY, 2019.

[9] A. Boyde and S. J. Jones, "Scanning electron microscopy of bone: instrument, specimen, and issues," *Microscopy Research and Technique*, vol. 33, no. 2, pp. 92–120, 1996.

[10] S. J. Jones, A. Boyde, N. N. Ali, and E. Maconnachie, "A review of bone cell and substratum interactions: an illustration of the role of scanning electron microscopy," *Scanning*, vol. 7, no. 1, p. 24, 1985.

[11] A. Boyde and M. H. Hobdell, "Scanning electron microscopy of lamellar bone," *Zeitschrift für Zellforschung und Mikroskopische Anatomie*, vol. 93, no. 2, pp. 213–231, 1968.

[12] M. Relucenti, S. Miglietta, E. Covelli et al., "Ciliated cell observation by SEM on the surface of human incudo-malleolar-joint articular cartilage: are they a new chondrocyte phenotype?," *Acta Oto-Laryngologica*, vol. 139, no. 5, pp. 439–443, 2019.

[13] G. Familiari, A. Familiari, G. Macchiarelli, L. J. A. DiDio, and P. M. Motta, "The use of sonic frequencies as a clearing agent of specimens to be observed with scanning electron microscopy," *Scanning Microscopy*, vol. 7, no. 1, pp. 107–114, 1993.

[14] D. W. Dempster, E. Shane, W. Horbert, and R. Lindsay, "A simple method for correlative light and scanning electron microscopy of human iliac crest bone biopsies: qualitative observations in normal and osteoporotic subjects," *Journal of Bone and Mineral Research*, vol. 1, no. 1, pp. 15–21, 1986.

[15] S. Ren, H. Takano, and K. Abe, "Two types of bone resorption lacunae in the mouse parietal bones as revealed by scanning electron microscopy and histochemistry," *Archives of Histology and Cytology*, vol. 68, no. 2, pp. 103–113, 2005.

[16] H. Hashizume, K. Abe, and T. Ushiki, "Detection of mineral density on the surface of mouse parietal bones: backscattered electron imaging of low accelerating voltage scanning electron microscopy," *Archives of Histology and Cytology*, vol. 60, no. 2, pp. 195–204, 1997.

[17] R. J. Murrills, E. Shane, R. Lindsay, and D. W. Dempster, "Bone resorption by isolated human osteoclasts in vitro: effects of calcitonin," *Journal of Bone and Mineral Research*, vol. 4, no. 2, pp. 259–268, 1989.

[18] B. R. McCreadie, S. J. Hollister, M. B. Schaffler, and S. A. Goldstein, "Osteocyte lacuna size and shape in women with and without osteoporotic fracture," *Journal of Biomechanics*, vol. 37, no. 4, pp. 563–572, 2004.

[19] B. Alexander, T. L. Daulton, G. M. Genin et al., "The nanometre-scale physiology of bone: steric modelling and scanning transmission electron microscopy of collagen-mineral structure," *Journal of The Royal Society Interface*, vol. 9, no. 73, pp. 1774–1786, 2012.

[20] N. Kourkoumelis, I. Balatsoukas, and M. Tzaphlidou, "Ca/P concentration ratio at different sites of normal and osteoporotic rabbit bones evaluated by Auger and energy dispersive X-ray spectroscopy," *Journal of Biological Physics*, vol. 38, no. 2, pp. 279–291, 2012.

[21] V. Cottignoli, M. Relucenti, G. Agrosì et al., "Biological niches within human calcified aortic valves: towards understanding of the pathological biomineralization process," *BioMed Research International*, vol. 2015, 542610 pages, 2015.

[22] S. Xie, X. Wang, J. Ren, and W. Liu, "The role of bone resorption in the etiopathogenesis of acquired middle ear cholesteatoma," *European Archives of Oto-Rhino-Laryngology*, vol. 274, no. 5, pp. 2071–2078, 2017.

[23] W. J. Boyle, W. S. Simonet, and D. L. Lacey, "Osteoclast differentiation and activation," *Nature*, vol. 423, no. 6937, pp. 337–342, 2003.

[24] S. L. Teitelbaum and F. P. Ross, "Genetic regulation of osteoclast development and function," *Nature Reviews. Genetics*, vol. 4, no. 8, pp. 638–649, 2003.

[25] K. W. Kim, M. L. Cho, S. H. Lee et al., "Human rheumatoid synovial fibroblasts promote osteoclastogenic activity by activating RANKL via TLR-2 and TLR-4 activation," *Immunology Letters*, vol. 110, no. 1, pp. 54–64, 2007.

[26] H. Takayanagi, H. Iizuka, T. Juji et al., "Involvement of receptor activator of nuclear factor kappaB ligand/osteoclast differentiation factor in osteoclastogenesis from synoviocytes in rheumatoid arthritis," *Arthritis and Rheumatism*, vol. 43, no. 2, pp. 259–269, 2000.

[27] I. B. Mcinnes and G. Schett, "The pathogenesis of rheumatoid arthritis," *The New England Journal of Medicine*, vol. 365, no. 23, pp. 2205–2219, 2011.

[28] G. Mbalaviele, D. V. Novack, G. Schett, and S. L. Teitelbaum, "Inflammatory osteolysis: a conspiracy against bone," *The Journal of Clinical Investigation*, vol. 127, no. 6, pp. 2030–2039, 2017.

[29] T. T. Jung and S. K. Juhn, "Prostaglandins in human cholesteatoma and granulation tissue," *The American Journal of Otology*, vol. 9, no. 3, pp. 197–200, 1988.

[30] J. Kuczkowski, M. Sakowicz-Burkiewicz, E. Iżycka-Świeszewska, B. Mikaszewski, and T. Pawełczyk, "Expression of tumor necrosis factor-α, interleukin-1α, interleukin-6 and interleukin-10 in chronic otitis media with bone osteolysis," *ORL*, vol. 73, no. 2, pp. 93–99, 2011.

[31] R. F. Vitale and F. de Andrade Quintanilha Ribeiro, "The role of Tumor Necrosis Factor -Alpha (TNF-α) in bone resorption present in middle ear cholesteatoma," *Brazilian Journal of Otorhinolaryngology*, vol. 73, no. 1, pp. 117–121, 2007.

[32] W. Likus, K. Siemianowicz, J. Markowski et al., "Bacterial infections and osteoclastogenesis regulators in men and women with cholesteatoma," *Archivum Immunologiae et Therapiae Experimentalis*, vol. 64, no. 3, pp. 241–247, 2016.

[33] F. A. W. Peek, M. A. Huisman, R. J. Berckmans, A. Sturk, J. van Loon, and J. J. Grote, "Lipopolysaccharide concentration and bone resorption in cholesteatoma," *Otology & Neurotology*, vol. 24, no. 5, pp. 709–713, 2003.

[34] S. Yetiser, B. Satar, and N. Aydin, "Expression of epidermal growth factor, tumor necrosis factor-alpha, and interleukin-1alpha in chronic otitis media with or without cholesteatoma," *Otology & Neurotology*, vol. 23, no. 5, pp. 647–652, 2002.

[35] P. M. Motta, P. M. Andrews, and K. R. Porter, Eds., *Microanatomy of cell and tissue surfaces. An atlas of scanning electron microscopy*, Lea & Febiger, Philadelphia, 1977.

[36] D. W. Fawcett, Ed., *The Cell*, W.B. Saunders, Philadelphia, 1981.

[37] P. M. Motta, Ed., "Cells and Tissues, A three-dimensional approach by modern techniques in microscopy," in *Prog. Clin. Biol. Res.*, vol. 295, Alan R. Liss, Inc., New York, 1989.

[38] J. H. Shim, Z. Stavre, and E. M. Gravallese, "Bone loss in rheumatoid arthritis: basic mechanisms and clinical implications," *Calcified Tissue International*, vol. 102, no. 5, pp. 533–546, 2018.

Hindawi
Scanning
Volume 2019, Article ID 1289570, 6 pages
https://doi.org/10.1155/2019/1289570

Research Article

Trueness and Precision of Two Intraoral Scanners: A Comparative In Vitro Study

Raul Nicolae Rotar,[1] Anca Jivanescu,[1] Codruta Ille,[1] Angela Codruta Podariu,[2] Daniela Elisabeta Jumanca,[2] Ana-Maria Matichescu,[2] Octavia Balean,[2] and Laura Cristina Rusu[3]

[1]*Department of Prosthodontics, University of Medicine and Pharmacy "Victor Babes", Timisoara, B-dul Revolutiei 1989, No 9, 300580, Romania*
[2]*Department of Preventive Dentistry, Community and Oral Health, University of Medicine and Pharmacy "Victor Babes", Timisoara, Splaiul Tudor Vladimirescu, nr.14 A, 300174, Romania*
[3]*Department of Oral Pathology, University of Medicine and Pharmacy "Victor Babes", Timisoara, Splaiul Tudor Vladimirescu, nr.14 A, 300174, Romania*

Correspondence should be addressed to Anca Jivanescu; ajivanescu@yahoo.com

Received 8 August 2019; Accepted 24 September 2019; Published 21 October 2019

Academic Editor: Andrea Picone

The aim of this study was to evaluate the accuracy of two intraoral scanners used in the dental office. A molar fixed in a typodont was prepared for a ceramic onlay. The preparation was scanned using a high-resolution scanner (reference scanner) and saved as stereolithography (STL) format. The prepared resin molar was scanned again using the intraoral scanners, and all the scans were saved as well in STL format. All STL files were compared using metrology software (Geomagic Control X). Overlapping the meshes allowed the assessment of the scans in terms of trueness and precision. Based on the results of this study, the differences of trueness and precision between the intraoral scanners were minimal.

1. Introduction

Digital impressions are getting more and more importance in the dental office, leading to an increase in the number of intraoral scanners available on the market [1–5], and as a result, many clinicians may have second thoughts when choosing the most suitable intraoral system for their work [2, 6].

The main advantages that these systems provide over the conventional impression are the comfort for the patient, time efficiency, and also the reduced costs [7, 8]. Also, the possibility of immediate control of the impression and basically "indestructible" 3D models that can be stored indefinitely add up to the scale in favor of digital impression procedures [9–11].

The way a scanner works is by measuring the reflection times of a surface and based on an algorithm it "attaches" the images that it records. Even if the digital impression procedure is not very complicated, the working algorithm is complex [1]. The scanner's software generates point clouds and meshes that reconstruct the scanned surface using a powerful processing software that allows for high-quality 3D models [12, 13].

A number of studies have shown that intraoral scanners are a reliable way of recording tooth preparations whether they are single crowns, inlays, onlays, implants [14–16], or fixed partial dentures [17–19].

When comparing digital impression accuracy, there are two aspects that are taken into consideration: trueness and precision. These variables are independent and do not reflect the same thing [13, 14]. Trueness shows how similar is a measurement to the value of the measured quantity. On the other hand, precision shows how much similar are repeated measurements, in other words the reproducibility of the impression [13–15]. As a result, the ideal intraoral scanner should have high trueness and also high precision.

The most common way of measuring the accuracy or either conventional or digital impressions is by comparing a reference scan, usually obtained by scanning a physical model with a desktop or an industrial scanner, and the resulting STL file is then compared with the test scan groups [20–24].

Due to the fact that there is no standardized method of scanning and the acquisition techniques for the IOS differ from one system to another, the analysis of the resulting meshes may prove difficult [21, 25].

A precise fit is extremely important when referring to long-lasting dental restorations. As a result, the impression process becomes a key step in determining the success of a treatment. A precise impression allows for a clear identification of the finish line which translates into a suitable emergence profile [26–29].

The aim of this study was to compare the accuracy (trueness and precision) of two intraoral scanners on an onlay preparation and to assess if there are any major discrepancies between the qualities of the final digital impressions.

2. Material and Methods

Two intraoral scanners Planmeca PlanScan (E4D Technologies, LLC, Richardson, TX, USA) and CEREC Omnicam (Sirona, Bensheim, Germany) and a high-resolution desktop scanner D700 (3Shape, Copenhagen, Denmark) were used in this study.

The Planmeca PlanScan works under the principle of optical coherence tomography and confocal microscopy. It is a powder-free scanner with a blue light real-time laser video streaming technology. It has tips of various dimensions with built-in heated mirrors. Planmeca PlanScan is an open system, since it allows conversion of the acquired proprietary files into STL files, readable by all CAD systems. It can be easily connected to a laptop via a USB port and has a proprietary milling machine available for the fabrication of full in-office digital restorations such as inlays, onlays, crowns, bridges, and veneers.

CEREC Omnicam is a structured light scanner that uses a white LED, and it works under the principle of optical triangulation and confocal microscopy. It is fast, it does not require powder, and it offers true color information. The tip is not too big; therefore, it is easier to scan the posterior areas. The digital workflow can take place directly at the chairside, using the proprietary CAD software, or via the cloud-based platform. CEREC Omnicam is also an open system allowing transformation of proprietary files into STL files, usable from any CAD system. The CAD/CAM system of Sirona allows the design and milling of prosthetic restorations and frameworks (inlays, onlays, veneers, crowns, bridges, and bars).

D700 is a desktop scanner that uses two cameras with reduced angle that allows the scanning of deep preparations and undercuts. It has a high accuracy (<20 microns) and is material color independent.

A standard resin upper first molar was prepared for a ceramic onlay. Next, the model was digitized using a desktop scanner (D700, 3Shape) in order to obtain a reference model. First, the prepared tooth was removed from the typodont and scanned individually followed by another scan with the adjacent teeth that later served in the alignment process. The 3-axis motion system facilitated easy object placement allowing the object to be tilted, rotated, and translated so as to be scanned from any viewpoint, making 3-axis the optimal number of axis for a scanning volume corresponding to a dental model. In the final processing step, the point cloud obtained from all views was converted into a 3D surface of fine triangles and the resulting data saved as a STL file (Figure 1).

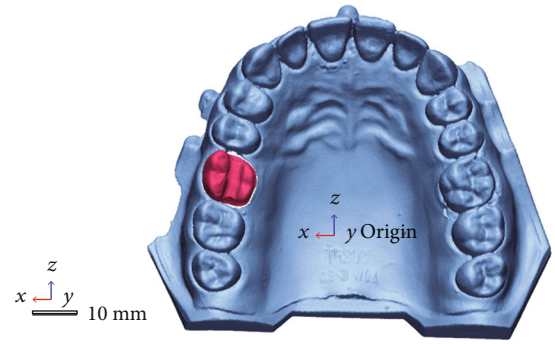

Figure 1: Reference model.

The same prepared molar was scanned ten times using two high-end intraoral scanners. The first five scans were taken with the scanner from Planmeca PlanScan and the rest up to ten with the Omnicam from CEREC. A specific scanning pattern was followed for all the scans starting from the mesial part of the occlusal surface of the preparation and then transitioning to the palatal surface followed by the distal part of the occlusal surface and in the end the transition to the buccal side of the prepared tooth, all in a continuous motion. All files were saved in STL format as well and used later on for a comparison in terms of trueness and precision (Figure 2).

Trueness values were obtained by superimposing the STL files from the test groups with the STL file from the reference scan. Overlapping the STL files within each group generated the precision values. Two random scans from each intraoral system were chosen and compared with all the other meshes from within each group. All scanning data and computations were performed using metrology software (Geomagic Control X). Using reverse engineering, the STL files were uploaded into the program and the models were trimmed, and only the prepared tooth data was analyzed. The STL file from the desktop scanner was set as the reference. The 3D models from the intraoral scanners were superimposed in the beginning using a rough "initial alignment" followed by a "best fit algorithm" that determined the final overlapping of the meshes (Figure 3). The resulting color map of the analyzed meshes was set between ±50 μm. The distances between different planes were color-coded, and the overall color map was generated based on these deviations.

For each set of scans, the mean and standard deviation values were calculated. The blue color indicated the inward displacement, and the red color showed the outward position of the mesh compared to the reference while the green color showed the absence of change (Figure 4).

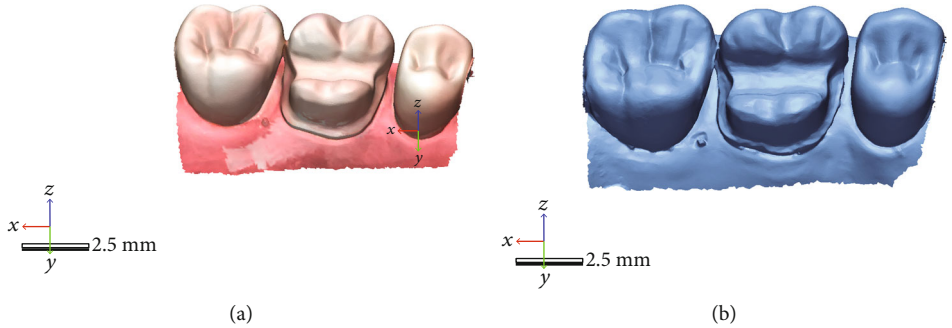

Figure 2: Intraoral scans with PlanScan (b) and Omnicam (a).

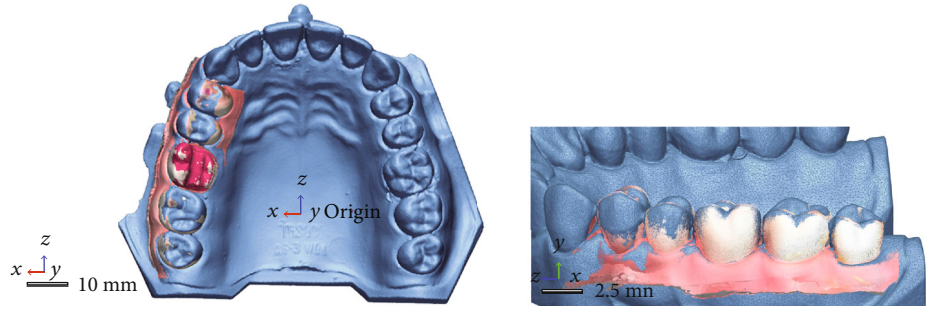

Figure 3: Alignment process of the meshes.

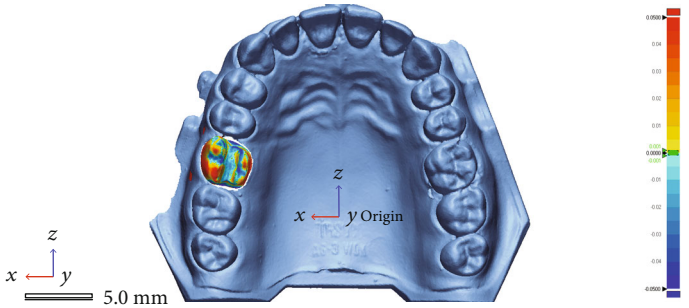

Figure 4: Color map of the deviation on the interest area.

Statistical analysis was preformed using the Kolmogorov-Smirnov test to assess data distribution.

Overall trueness and precision of the scanners were analyzed and compared, and the statistical significance was calculated using the paired t-test.

3. Results

The trueness and precision values of the two intraoral scanners for the onlay preparation are presented in Tables 1 and 2, respectively.

The mean trueness value of 48.6 ± 4.39 μm showed that the PlanScan scans had the best overall results. Regarding the precision of the two intraoral scanners, PlanScan also showed better results with a mean value of 24.86 ± 2.91 μm.

The p values for both trueness and precision were >0.05, indicating that there was no difference between the scanners.

The single best results for trueness and precision (visual color map representation) obtained with each device are presented in Figures 5–8.

4. Discussions

Clinical practice in dentistry is changing at an incredible pace due to the developments that take place in the software (computer assisted design) and hardware (milling machines and scanning tips) fields [1, 3, 5]. Optical impressions enhance the workflow in the dental office that leads to more predictable results, allowing for real-time adjustments of the impressions and when needed corrections of the prepared tooth areas [3, 9].

With so many intraoral scanners available on the market, little is known about the accuracy (trueness and precision) of these devices [10, 12]. A number of studies have

Table 1: Trueness values (μm) of the intraoral scanners (p value = 0.2).

	M1	M2	M3	M4	M5	Mean ± SD
Planmeca PlanScan	43 μm	53 μm	46 μm	53 μm	48 μm	48.6 ± 4.39 μm
CEREC Omnicam	54 μm	53 μm	46 μm	50 μm	62 μm	53 ± 5.91 μm

Table 2: Precision values (μm) of the intraoral scanners (p value = 0.08).

	M1	M2	M3	M4	M5	M6	M7	Mean ± SD
Planmeca PlanScan	28 μm	25 μm	21 μm	28 μm	22 μm	27 μm	23 μm	24.86 ± 2.91 μm
CEREC Omnicam	31 μm	31 μm	55 μm	21 μm	39 μm	28 μm	44 μm	35.57 ± 11.34 μm

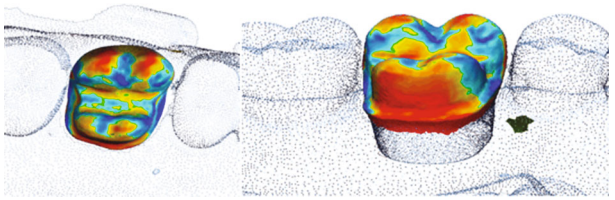

Figure 5: Color map of the PlanScan trueness deviation values around the interest area.

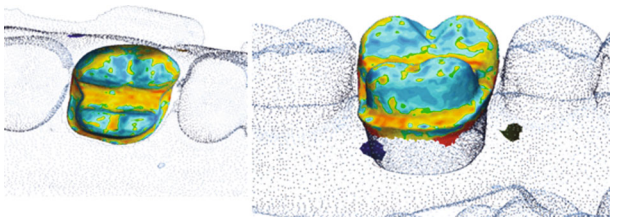

Figure 6: Color map of the Omnicam trueness deviation values around the interest area.

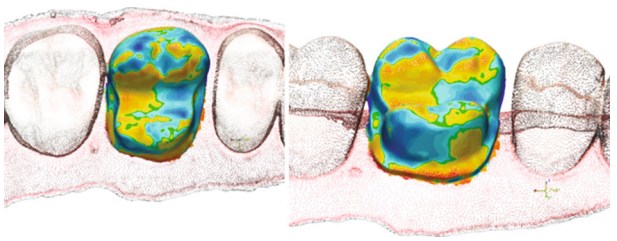

Figure 7: Color map of the PlanScan precision deviation values around the interest area.

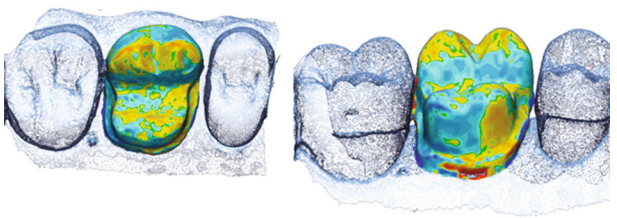

Figure 8: Color map of the Omnicam precision deviation values around the interest area.

shown that even if intraoral scanners are a reliable way of recording tooth preparations, it is not clear if they can completely replace the conventional impression in all treatment plans [15–17].

Nedelcu et al. assessed the accuracy of four intraoral scanners and concluded that these devices should be used only in particular scenarios that include smaller prosthetic treatments [21].

Similar conclusions were drawn by Schaefer et al. who measured the marginal fit of partial ceramic crowns and showed that even if the marginal gap distances were acceptable, there were important differences between the scanning systems [30].

Andriessen et al. also measured and compared the accuracy of three intraoral scanners for 3 implants on an edentulous ridge. The conclusion of the study was that the errors are directly proportional with the size of the scanned surface [15].

Our study has a number of limitations. Being an *in vitro* study, aspects that can influence the final accuracy of the digital impression such as humidity, saliva, blood, patient's movements, or the space for the scanning tip were not taken into consideration.

As a result, the observations of this study may be subject to change as the developing companies are investing more and more for the improvement of the data acquisition of these intraoral scanning systems.

5. Conclusions

This study compared the trueness and precision of two intraoral scanners in the scenario of an onlay on a complete dentate arch. The accuracy deviations of the analyzed scanners were consistent and with no major differences between them. Even if there were some deviations in visual inspection of the meshes, there was no statistical significance between the two intraoral scanners. More *in vivo* and *in vitro* studies are necessary for a clear validation of these results.

Data Availability

All data is available upon request.

Conflicts of Interest

The authors declare that there is no conflict of interests regarding the publication of this paper.

References

[1] S. Ting-shu and S. Jian, "Intraoral digital impression technique: a review," *Journal of Prosthodontics*, vol. 24, no. 4, pp. 313–321, 2015.

[2] M. Zimmermann, A. Mehl, W. H. Mörmann, and S. Reich, "Intraoral scanning systems – a current overview," *International Journal of Computerized Dentistry*, vol. 18, no. 2, pp. 101–129, 2015.

[3] W. H. Moörmann, "The evolution of the CEREC system," *The Journal of the American Dental Association*, vol. 137, pp. 7S–13S, 2006.

[4] W. H. Mörmann and A. Bindl, "The Cerec 3–a quantum leap for computer-aided restorations: initial clinical results," *Quintessence International*, vol. 31, no. 10, pp. 699–712, 2000.

[5] W. Renne, M. Ludlow, J. Fryml et al., "Evaluation of the accuracy of 7 digital scanners: an in vitro analysis based on 3-dimensional comparisons," *The Journal of Prosthetic Dentistry*, vol. 118, no. 1, pp. 36–42, 2017.

[6] S. Logozzo, E. M. Zanetti, G. Franceschini, A. Kilpela, and A. Makynen, "Recent advances in dental optics - part I: 3D intraoral scanners for restorative dentistry," *Optics and Lasers in Engineering*, vol. 54, no. 3, pp. 203–221, 2014.

[7] E. Yuzbasioglu, H. Kurt, R. Turunc, and H. Bilir, "Comparison of digital and conventional impression techniques: evaluation of patients' perception, treatment comfort, effectiveness and clinical outcomes," *BMC Oral Health*, vol. 14, no. 1, 2014.

[8] U. Schepke, H. J. A. Meijer, W. Kerdijk, and M. S. Cune, "Digital versus analog complete-arch impressions for single-unit premolar implant crowns: operating time and patient preference," *The Journal of Prosthetic Dentistry*, vol. 114, no. 3, pp. 403–406.e1, 2015.

[9] S. B. M. Patzelt, C. Lamprinos, S. Stampf, and W. Att, "The time efficiency of intraoral scanners: an in vitro comparative study," *Journal of the American Dental Association*, vol. 145, no. 6, pp. 542–551, 2014.

[10] T. Grünheid, S. D. McCarthy, and B. E. Larson, "Clinical use of a direct chairside oral scanner: an assessment of accuracy, time, and patient acceptance," *American Journal of Orthodontics and Dentofacial Orthopedics*, vol. 146, no. 5, pp. 673–682, 2014.

[11] M. L. C. Aragón, L. F. Pontes, L. M. Bichara, C. Flores-Mir, and D. Normando, "Validity and reliability of intraoral scanners compared to conventional gypsum models measurements: a systematic review," *The European Journal of Orthodontics*, vol. 38, no. 4, pp. 429–434, 2016.

[12] B. Gjelvold, B. R. Chrcanovic, E. K. Korduner, I. Collin-Bagewitz, and J. Kisch, "Intraoral digital impression technique compared to conventional impression technique. A randomized clinical trial," *Journal of Prosthodontics*, vol. 25, no. 4, pp. 282–287, 2016.

[13] C. Goracci, L. Franchi, A. Vichi, and M. Ferrari, "Accuracy, reliability, and efficiency of intraoral scanners for full-arch impressions: a systematic review of the clinical evidence," *The European Journal of Orthodontics*, vol. 38, no. 4, pp. 422–428, 2016.

[14] J.-F. Güth, D. Edelhoff, J. Schweiger, and C. Keul, "A new method for the evaluation of the accuracy of full-arch digital impressions in vitro," *Clinical Oral Investigations*, vol. 20, no. 7, pp. 1487–1494, 2016.

[15] F. S. Andriessen, D. R. Rijkens, W. J. van der Meer, and D. W. Wismeijer, "Applicability and accuracy of an intraoral scanner for scanning multiple implants in edentulous mandibles: a pilot study," *The Journal of Prosthetic Dentistry*, vol. 111, no. 3, pp. 186–194, 2014.

[16] F. G. Mangano, G. Veronesi, U. Hauschild, E. Mijiritsky, and C. Mangano, "Trueness and precision of four intraoral scanners in oral implantology: a comparative *in vitro* study," *PLoS One*, vol. 11, no. 9, article e0163107, 2016.

[17] J. Ng, D. Ruse, and C. Wyatt, "A comparison of the marginal fit of crowns fabricated with digital and conventional methods," *The Journal of Prosthetic Dentistry*, vol. 112, no. 3, pp. 555–560, 2014.

[18] K. Ueda, F. Beuer, M. Stimmelmayr, K. Erdelt, C. Keul, and J. F. Guth, "Fit of 4-unit FDPs from CoCr and zirconia after conventional and digital impressions," *Clinical Oral Investigations*, vol. 20, no. 2, pp. 283–289, 2016.

[19] T. Abdel-Azim, K. Rogers, E. Elathamna, A. Zandinejad, M. Metz, and D. Morton, "Comparison of the marginal fit of lithium disilicate crowns fabricated with CAD/CAM technology by using conventional impressions and two intraoral digital scanners," *The Journal of Prosthetic Dentistry*, vol. 114, no. 4, pp. 554–559, 2015.

[20] F. Mangano, A. Gandolfi, G. Luongo, and S. Logozzo, "Intraoral scanners in dentistry: a review of the current literature," *BMC Oral Health*, vol. 17, no. 1, article 442, 2017.

[21] R. Nedelcu, P. Olsson, I. Nyström, J. Rydén, and A. Thor, "Accuracy and precision of 3 intraoral scanners and accuracy of conventional impressions: a novel in vivo analysis method," *Journal of Dentistry*, vol. 69, pp. 110–118, 2018.

[22] A. Ender and A. Mehl, "Accuracy of complete-arch dental impressions: a new method of measuring trueness and precision," *The Journal of Prosthetic Dentistry*, vol. 109, no. 2, pp. 121–128, 2013.

[23] A. S. K. Persson, A. Odén, M. Andersson, and G. Sandborgh-Englund, "Digitization of simulated clinical dental impressions: virtual three-dimensional analysis of exactness," *Dental Materials*, vol. 25, no. 7, pp. 929–936, 2009.

[24] A. Mehl, A. Ender, W. Mörmann, and T. Attin, "Accuracy testing of a new intraoral 3D camera," *International Journal of Computerized Dentistry*, vol. 12, no. 1, pp. 11–28, 2009.

[25] J. J. Lee, I. I. D. Jeong, J. Y. Park, J. H. Jeon, J. H. Kim, and W. C. Kim, "Accuracy of single-abutment digital cast obtained using intraoral and cast scanners," *The Journal of Prosthetic Dentistry*, vol. 117, no. 2, pp. 253–259, 2017.

[26] A. Keeling, J. Wu, and M. Ferrari, "Confounding factors affecting the marginal quality of an intra-oral scan," *Journal of Dentistry*, vol. 59, pp. 33–40, 2017.

[27] P. Svanborg, H. Skjerven, P. Carlsson, A. Eliasson, S. Karlsson, and A. Örtorp, "Marginal and internal fit of cobalt-chromium fixed dental prostheses generated from digital and conventional impressions," *International Journal of Dentistry*, vol. 2014, Article ID 534382, 9 pages, 2014.

[28] E. Anadioti, S. A. Aquilino, D. G. Gratton et al., "3D and 2D marginal fit of pressed and CAD/CAM lithium disilicate crowns made from digital and conventional impressions," *Journal of Prosthodontics*, vol. 23, no. 8, pp. 610–617, 2014.

[29] P. Tsirogiannis, D. R. Reissmann, and G. Heydecke, "Evaluation of the marginal fit of single-unit, complete-coverage ceramic restorations fabricated after digital and conventional impressions: a systematic review and meta-analysis," *The Journal of Prosthetic Dentistry*, vol. 116, no. 3, pp. 328–335.e2, 2016.

[30] O. Schaefer, M. Decker, F. Wittstock, H. Kuepper, and A. Guentsch, "Impact of digital impression techniques on the adaption of ceramic partial crowns in vitro," *Journal of Dentistry*, vol. 42, no. 6, pp. 677–683, 2014.

Hindawi
Scanning
Volume 2019, Article ID 4274715, 14 pages
https://doi.org/10.1155/2019/4274715

Research Article

Combining Intraoral and Face Scans for the Design and Fabrication of Computer-Assisted Design/Computer-Assisted Manufacturing (CAD/CAM) Polyether-Ether-Ketone (PEEK) Implant-Supported Bars for Maxillary Overdentures

Francesco Mangano,[1] **Carlo Mangano**,[2] **Bidzina Margiani**,[1] **and Oleg Admakin**[3]

[1]*Lecturer, Department of Prevention and Communal Dentistry, Sechenov First Moscow State Medical University, 119992 Moscow, Russia*
[2]*Professor and Lecturer, Department of Dental Sciences, Vita and Salute University San Raffaele, 20132 Milan, Italy*
[3]*Professor and Head, Department of Prevention and Communal Dentistry, Sechenov First Moscow State Medical University, 119992 Moscow, Russia*

Correspondence should be addressed to Francesco Mangano; francescomangano1@mclink.net

Received 20 June 2019; Accepted 1 July 2019; Published 22 August 2019

Guest Editor: Lavinia C. Ardelean

Purpose. To present a digital method that combines intraoral and face scanning for the computer-assisted design/computer-assisted manufacturing (CAD/CAM) fabrication of implant-supported bars for maxillary overdentures. *Methods*. Over a 2-year period, all patients presenting to a private dental clinic with a removable complete denture in the maxilla, seeking rehabilitation with implants, were considered for inclusion in this study. Inclusion criteria were fully edentulous maxilla, functional problems with the preexisting denture, opposing dentition, and sufficient bone volume to insert four implants. Exclusion criteria were age < 55 years, need for bone augmentation, uncompensated diabetes mellitus, immunocompromised status, radio- and/or chemotherapy, and previous treatment with oral and/or intravenous aminobisphosphonates. All patients were rehabilitated with a maxillary overdenture supported by a CAD/CAM polyether-ether-ketone (PEEK) implant-supported bar. The outcomes of the study were the passive fit/adaptation of the bar, the 1-year implant survival, and the success rates of the implant-supported overdentures. *Results*. 15 patients (6 males, 9 females; mean age 68.8 ± 4.7 years) received 60 implants and were rehabilitated with a maxillary overdenture supported by a PEEK bar, designed and milled from an intraoral digital impression. The intraoral scans were integrated with face scans, in order to design each bar with all available patient data (soft tissues, prosthesis, implants, and face) in the correct spatial position. When testing the 3D-printed resin bar, 12 bars out of 15 (80%) had a perfect passive adaptation and fit; in contrast, 3 out of 15 (20%) did not have a sufficient passive fit or adaptation. No implants were lost, for a 1-year survival of 100% (60/60 surviving implants). However, some complications (two fixtures with peri-implantitis in the same patient and two repaired overdentures in two different patients) occurred. This determined a 1-year success rate of 80% for the implant-supported overdenture. *Conclusions*. In this study, the combination of intraoral and face scans allowed to successfully restore fully edentulous patients with maxillary overdentures supported by 4 implants and a CAD/CAM PEEK bar. Further studies are needed to confirm these outcomes.

1. Introduction

The digital revolution is changing the world of dentistry [1]. Intraoral scanners (IOSs) [2, 3], face scanners (FSs) [4, 5], and cone beam computed tomography (CBCT) [6] allow the dentist to capture three-dimensional (3D) information about the patient and, from such data acquisition, create virtual models of teeth, face, and bone bases. These data are then imported into specific computer-assisted design (CAD) software and superimposed upon each other in order to obtain

the "virtual patient" [7, 8], the starting point for 3D surgical, prosthetic, and orthodontic planning. Within the CAD software, the dentist and dental technician plan the therapy and design a series of devices (surgical templates [9, 10], prostheses [11–13], and orthodontic devices [14]) to be used on patients. Finally, these devices are processed by appropriate computer-assisted manufacturing (CAM) software, milled or 3D printed, and are available for clinical use [15].

In the prosthetic field, the digital revolution has a strong impact because the dentist can capture optical impressions with IOS [2, 3, 11–13]; these impressions are used by the dental technician for the planning and hence the production of a whole series of fixed prosthetic restorations (inlays [12, 16], onlays [16], single crowns [17, 18], and bridges of up to 4 or 5 elements [19]). The literature now shows that all these applications are possible and represent a clinical reality [11]. Patients favor optical impressions, which have eliminated the need for conventional analog impressions with trays and materials (alginate, polyvinylsiloxane, and polyether) [2, 20, 21]. The optical impressions also eliminate the discomfort linked to the conventional analog impressions; they are easy to capture for the clinician (even in the presence of undercuts or dental implants), and they can be sent directly to the dental laboratory by e-mail, at no cost [2, 20]. The dental technician can view the impressions and immediately give feedback to the clinician, while the patient sits comfortably in the dental chair. Furthermore, the high quality of the 3D images derived from the optical impressions even makes the IOS useful as a marketing tool with patients.

Although IOSs are becoming widespread and have become a very useful tool for capturing impressions in partially edentulous patients [2, 11–19], the scientific literature does not seem to support their use in completely edentulous patients [22–24]. Numerous systematic reviews suggest that IOSs do not yet have adequate accuracy to allow CAD and thus the fabrication of full-arch-type restorations [22–24], particularly in patients with implants [23, 24]; in this, the distance between the implants seems to play a major role [25].

However, data emerging from these revisions stem from the analysis of previous clinical trials, in which first-generation IOSs were used [22–24]. The technological evolution is proceeding very fast, and the manufacturing companies release new hardware and software every month to improve the accuracy of their IOS; scientific literature has different times and struggles to follow. Furthermore, it must be emphasized that there are statistically significant differences in the accuracy of different IOSs, especially in scans of completely edentulous patients [3, 26]. Moreover, the restoration of the completely edentulous patient can take place with a fixed prosthesis supported by 6–8 implants [27, 28], such as with a bar-retained overdenture supported by 4 implants [29]; in the latter application, the implants are closer to each other, generally inserted into the anterior area of the maxilla, in which case the optical impression can be less difficult.

Recently, in fact, some clinical studies have shown that using the latest-generation IOS, it is possible to design and fabricate clinically precise CAD/CAM implant-supported bars [30, 31]. Today, this is possible and represents an important step forward in the field of digitalization of prosthetic procedures within the dental practice; it is in fact possible to plan the shape and volume of the bar according to the prosthetic spaces available [30, 31]. In this context, the acquisition of the patient's face via FS represents a further important development, not only to facilitate the modeling of the bar in relation to tissue volumes but also to present the case to the patient.

The aim of the present prospective clinical study is to present a digital method that combines intraoral and face scanning for the CAD/CAM fabrication of implant-supported bars for maxillary overdentures.

2. Materials and Methods

2.1. Patient Selection. Over a 2-year period (2017–2018), all patients presenting to a private dental clinic, and seeking prosthetic rehabilitation with implants, were considered for inclusion in this prospective clinical study. Inclusion criteria for enrollment in the study were (1) fully edentulous maxilla; (2) functional problems with the complete removable denture (e.g., lack of stability, discomfort due to the size of the prosthesis); (3) presence of opposing natural or artificial dentition in the antagonist arch; (4) sufficient bone volume to be able to insert four implants of standard diameter and length (at least 3.3 mm × 10 mm), suitable for supporting a bar, in the anterior maxilla; and (5) good general health status. Exclusion criteria for enrollment in this study were (1) age < 55 years; (2) previous bone augmentation techniques and/or regenerative bone procedures or need to proceed with them, in order to be able to insert dental implants; (3) uncompensated diabetes mellitus; (4) immunocompromised status; (5) radio- and/or chemotherapy; and (6) treatment with aminobisphosphonates (taken orally or parenterally). The patients who presented with the conditions listed in the inclusion criteria, and who did not have any of those listed in the exclusion criteria, were informed in detail about the possible therapeutic strategies (fixed prosthesis supported by 6–8 implants or bar-supported overdenture sustained by 4 implants) as well as their advantages and limitations. At the end of the informational interview, all patients who opted for rehabilitation with bar-retained overdentures were included in the present clinical study. Before starting the treatment, all the enrolled patients were informed of the importance of avoiding smoking, since smoke represents a risk factor for implant failure in the short and long term [32]. In addition, they received detailed information on the potential risks related to the implant treatment and signed an informed consent and an authorization for inclusion in the study. This study was approved by the Ethics Committee of Sechenov First Moscow State Medical University and was conducted in accordance with the principles set out in the 1975 Helsinki Declaration on clinical research involving humans, as revised in 2008.

2.2. Clinical and Laboratory Procedures. The surgery took place under local anesthesia, as previously described [29], by raising a full thickness flap and inserting 4 implants in

the anterior area of the maxilla. The tapered implants used in this study (BTSafe®, BTK, Dueville, Vicenza, Italy) were characterized by double-lead threads with a hexagonal conical connection (11°) and integrated platform switching [33]. The dual acid-etched surface of these implants was the result of treatment with a strong inorganic acid mixture (H_2SO_4, H_3PO_4, HCl, and HF), giving the following roughness parameters: $Ra = 1.12\,(60.41)\,\mu m$, $Rq = 1.34\,(60.69)\,\mu m$, and $Rt = 3.86\,(61.40)\,\mu m$ [34]. The implants were available in different diameters (3.3, 3.75, 4.1, and 4.8 mm) and lengths (8, 10, 12, and 14 mm). Once the implants were inserted and the sutures placed, the preexisting denture was discharged abundantly in the area of the implants (to avoid overloading), relined, and functionalized. The preexisting denture was carefully relined after functionalization and was therefore extraorally scanned with a structured light IOS (CS 3600®, Carestream Dental, Atlanta, Georgia, USA). Care was taken to capture the entire body of the denture (Figures 1(a)–1(f)) and, with it, the indirect functionalized impression of all the mucosal tissues, up to the area of the fornix and muscle insertions. The .STL file of the preexisting, relined, and functionalized complete denture was then imported into a free CAD software (Meshmixer®, Autodesk, San Rafael, CA, USA), where it was prepared for printing. Then, a replica of the preexisting relined and functionalized denture was 3D printed in a proprietary opaque resin (PrecisaRD097®, DWS, Thiene, Vicenza, Italy) using a stereolithographic (SLA) 3D printer (3500PD®, DWS, Thiene, Vicenza, Italy) (Figures 2(a)–2(c)). This replica was manually opened and discarded in the anterior area, corresponding to the implant scanbodies (Figures 2(d) and 2(e)). One week later, the patient was recalled for a second appointment, in which intraoral scans were taken with the aforementioned structured light IOS. The intraoral scan was performed using the dedicated implant acquisition mode (Figures 3(a)–3(c)). The clinician used a zig-zag technique: he started from the buccal side, carried occlusal and then palatal, and then returned to the occlusal, progressing constantly. The movement described by the tip of the scanner was therefore an arc, moving slowly to fly over the teeth and scanbodies, capturing all details possible but only in the area of interest. The scan started with the antagonist arch; then the master model was scanned, in order to capture the mucosal collars of the implants after the removal of the healing screws. The master model scan was performed with the patient wearing the copy of the preexisting removable denture, properly opened/discarded in the anterior area, i.e., the area of the implants. In other words, the mucosal collars and the soft tissues of the anterior area were visible and captured, but at the same time, the presence of the copy of the preexisting removable denture allowed the capture of the bite (occlusion). By capturing the bite, it was possible to get adequate information on the original vertical dimension of occlusion of the patient, given by the preexisting removable denture. After the capture of the bite, the mucosal collars were selectively cancelled, using the dedicated tools of the scanner acquisition software, and the scanbodies were screwed onto the implants. Thus, the first scan was completed with the capture of all the scanbodies in position. In this scan too, the patient had the replica of the denture in-mouth. Finally, before discharging the patient, since in this work the prosthetic bases were manufactured analogically, alginate impressions were recorded for the preparation of the individual tray useful for precision impressions and for the preparation of the prosthetic wax try-ins, for registering the vertical dimension of occlusion. After this meeting, all .STL files derived from the intraoral scan were saved in a dedicated folder, in the correct reciprocal spatial position (Figure 4); then, the scan of the preexisting denture of the patient was aligned on the master intraoral scan without scanbodies, using the teeth as reference points, via reverse engineering software (Studio 2012®, Geomagic, Morrisville, NC, USA). The files were then ready to be imported into Meshmixer®. Within this software, the model file of the opposing arch was used as basis for designing and modeling of the individual reference tray (IRT). The IRT was a bite splint modeled on the anterior teeth of the antagonist arch and therefore individualized; it was designed to fit firmly on the patient's antagonist model; an extraoral reference plate was therefore connected to this bite splint. This plate had geometric shapes (square, triangle, and circle) of known dimensions and was provided free of charge by the manufacturer of the powerful face scanner (OBI®, Fifthingenium, Milan, Italy) later used in this protocol, as an essential component in the process of superimposition between face scans and intraoral scans. Within Meshmixer®, through a few simple steps, the clinician modeled this individualized bite splint and "attached" it to the extraoral reference plate, obtaining the IRT (Figures 5(a) and 5(b)). The IRT was correctly positioned on the antagonist model, and all the models were in the correct spatial relationship to each other. The .STL files of the models were saved in a dedicated folder, and the IRT file was ready for 3D printing. The IRT was printed with the aforementioned 3500PD® SLA 3D printer, using the same proprietary opaque resin of the denture replica (Figure 5(c)).

Once the IRT was ready, it was possible to recall the patient for the third appointment, in order to take the face scans of the patient, using the aforementioned face scanner (OBI®). The first face scan was captured with the smiling patient, without the IRT (Figure 6(a)). The second face scan was always carried out with the smiling patient, but with the IRT (Figures 6(b)–6(d)). In all, the two face scans took only 5 minutes and were performed with the scanner fixed on a tripod, and the patient in front of it, performing head movements, was guided by the acquisition software (turn left, right, up, and down). Both face scans were saved in .OBJ format and were ready for import into the prosthetic CAD software. All files (antagonist and master with copy of the preexisting complete removable denture opened in the anterior area, the latter with and without the scanbodies) deriving from Meshmixer®, along with the file IRT, were imported into a prosthetic CAD (Dentalcad®, Exocad, Darmstadt, Germany) for the modeling of the implant-supported bar, in respect of the correct spaces and prosthetic volumes. All files were in the correct reciprocal spatial position. At this point, the dental technician imported the face scans. The first face scan to be imported was the one with the IRT. This color texture, in .OBJ format, was superimposed on the CAD drawing

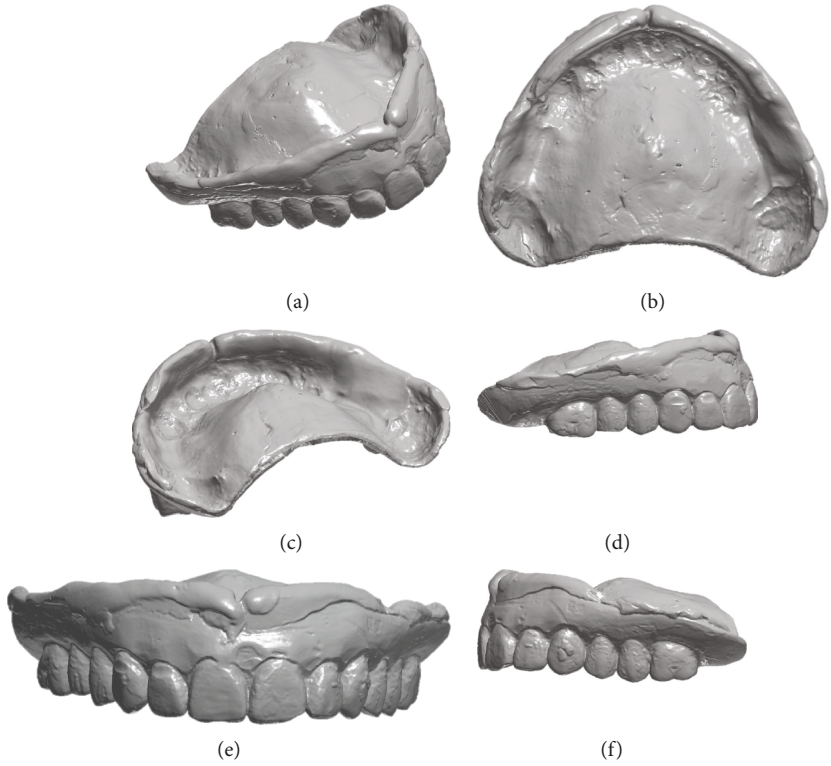

Figure 1: Extraoral scan of the preexisting complete removable denture, suitably relined with CS 3600® (Carestream Dental, Atlanta, GE, USA). (a) Anterior perspective view; (b) vision of the inner part in contact with the mucosal tissues; (c) posterior perspective view; (d) right side view; (e) front view; (f) left side view.

of the IRT; the overlap took place first by points, using the geometric references of the tray (Figures 7(a) and 7(b)), and then by surfaces, in order to obtain an ideal alignment. The moving object was, of course, the face scan. Immediately after, the second face scan (without IRT) was also imported. This scan was therefore aligned on the previous face scan, using the same method described above. The overlap by points was performed using stable morphometric landmarks (pupils, tip and wings of the nose, eyebrows, and tip of the chin) and was therefore perfected by the automatic superimposition algorithm (Figures 7(c) and 7(d)). At this point, the face scan of the patient without the tray was perfectly aligned with the models and the dental technician could model the bar having all the information useful for the project: master model with mucosal collars and scanbodies, antagonist, and face scan. The face scan could be eventually cut out in the smile area, in order to provide more details regarding the positioning of the underlying prosthetic components (Figures 8(a) and 8(b)). The dental technician proceeded to replace the meshes of the implant scanbodies with the corresponding library files and modeled the implant-supported maxillary bar (Figures 8(c) and 8(d)). In the present study, the implants inserted had a complete and integrated library that allowed rapid CAD modeling in the correct positions. The customized CAD/CAM bar was anatomically designed by an experienced dental technician according to the implant position and the shape and volume of the preexisting removable complete denture, taking into account the information obtained with the face scans. Four precision attachments (spheres) were planned along the implant bar. The .STL file of the bar (Figure 9) was then exported and printed in 3D with 3500PD® using a proprietary transparent resin (DS300®), in order to obtain a replica of the bar, useful for checking the intraoral passivity and fit of the structure. This bar was tested in the patient's mouth, to check the adaptation, precision, and passive fit of the structure. For testing, it was screwed on all four implants to verify the passive fit (Figures 10(a) and 10(b)). Then, the bar was unscrewed and the functional tray was relined in the patient's mouth using a dedicated impression material (Permlastic®, Kerr, Orange, CA, USA). The bar remained included in this impression. Moreover, the vertical dimension of occlusion was recorded by means of the wax try-ins. The lab poured a master cast and manufactured a wax copy of the final denture, mounted in an articulator, for the aesthetic and functional tests. When the quality of the test bar had been verified, and the functional and aesthetic tests were performed with the wax copy of the final denture, it was possible to proceed with the manufacture of the definitive bar in polyether-ether-ketone (PEEK). The bar was manufactured from a block of PEEK in a milling center using a 5-axis milling machine (DWX-51®, Roland Easy-Shape, Ascoli Piceno, Italy). The dental technician polished the bar and cemented the ball attachments, so the definitive bar could be tested in the mouth. Again, passive adaptation of the structure and closures was verified clinically, before and after screwing. The final PEEK bar was delivered (Figures 11(a)–11(c)) and screwed on the implants, together with the final denture (Figures 11(d)–11(f)). The occlusion

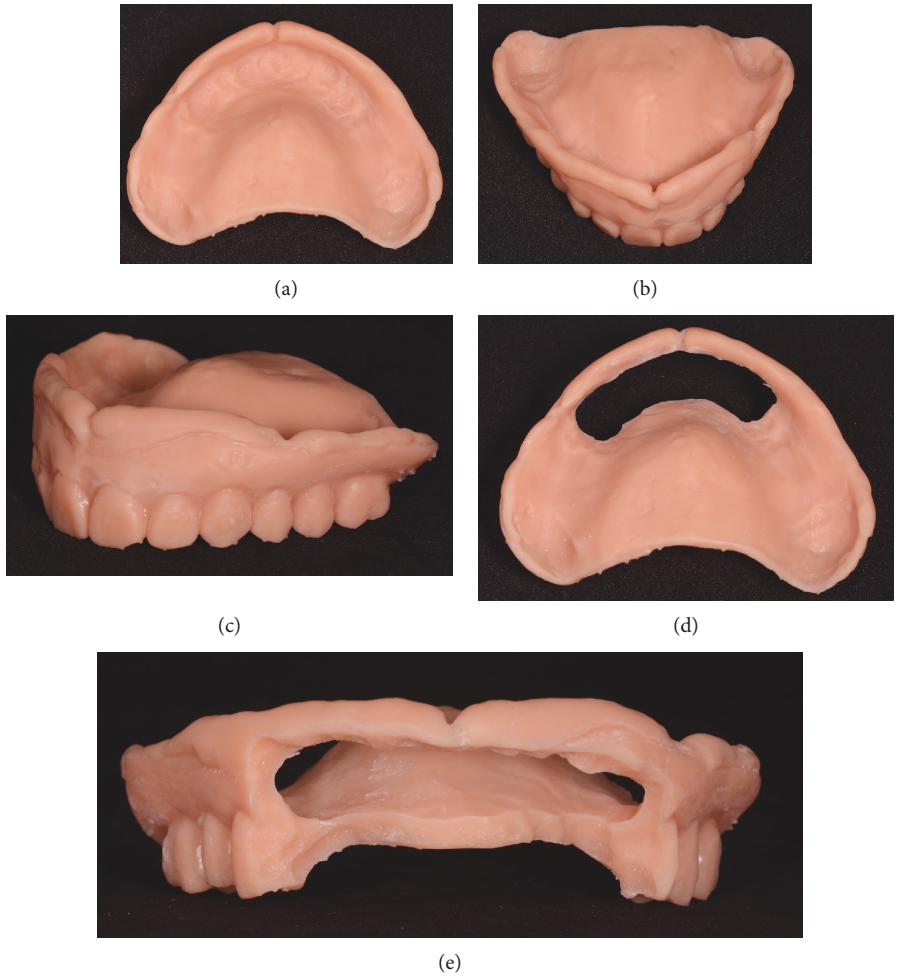

Figure 2: The copy of the preexisting complete removable denture, relined and extraorally scanned, is printed with a stereolithographic 3D printer (3500PD®, DWS, Thiene, Vicenza, Italy) and subsequently discarded and opened in the area of scanbodies. (a) Complete copy of the preexisting denture, internal view; (b) full copy of the preexisting denture, anterior view; (c) full copy of the preexisting denture, perspective view; (d) the copy of the preexisting denture discarded and opened in the anterior area, in correspondence with the emergencies of the scanbodies, internal view; (e) the copy of the preexisting denture in the anterior area, in correspondence with the emergencies of the scanbodies, frontal view.

and the aesthetic integration were carefully verified. The patients were enrolled in a standard implant recall program. Oral hygiene maintenance was checked and radiographs were taken 1 year after the implant placement.

2.3. Clinical Outcome Measures. The outcomes of the study were the adaptation/passive fit of the bar on the implants, the functional/aesthetic integration of the overdenture, the 1-year implant survival, and the success rates of the implant-supported overdenture.

2.3.1. Adaptation and Passive Fit of the Bar. The adaptation and passive fit of the bar were checked clinically, before and after screwing the replica (and the final bar) on the implants. The adaptation and passive fit were defined acceptable, in the absence of any movement of the bar before screwing, and when the bar was seated perfectly on the implants without any noticeable discrepancy. No difficulties were encountered when screwing the bar. In the case of movements of the bar during seating, or given evidence of discrepancies that could render the screwing on the implants difficult, the adaptation and passive fit were defined unacceptable, and so a new digital impression of the position of the implants, with and without scanbodies, had to be captured, in order to investigate the presence of any potential error(s) with the previous scan.

2.3.2. One-Year Implant Survival Rate. Implant mobility in the absence of clinical signs of infection, nontreatable peri-implant infection (with pain, suppuration, and bone loss), severe progressive marginal bone loss in the absence of infection, and implant body fracture were the conditions for which an implant could be removed and consequently defined as "failed." A distinction was made between "early" (within 3 months after implant placement) and "late" (at least 3 months after implant placement) failures. The 1-year implant survival rate was therefore calculated as the percentage of implant survival one year after placement. The implant survival rate was calculated at the patient level.

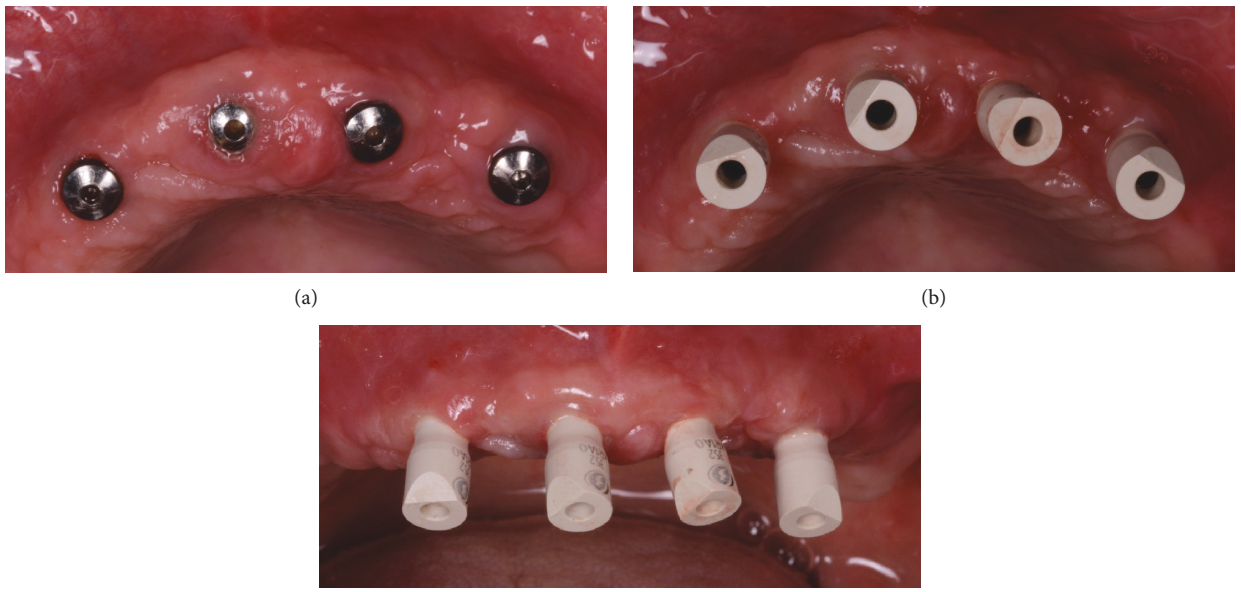

(a) (b)

(c)

Figure 3: Intraoral scanning clinical images. (a) The implants before the removal of healing abutments; (b) scanbodies (BTSafe® scan abutments, BTK, Dueville, Vicenza, Italy) in position, occlusal view; (c) scanbodies in position, frontal view.

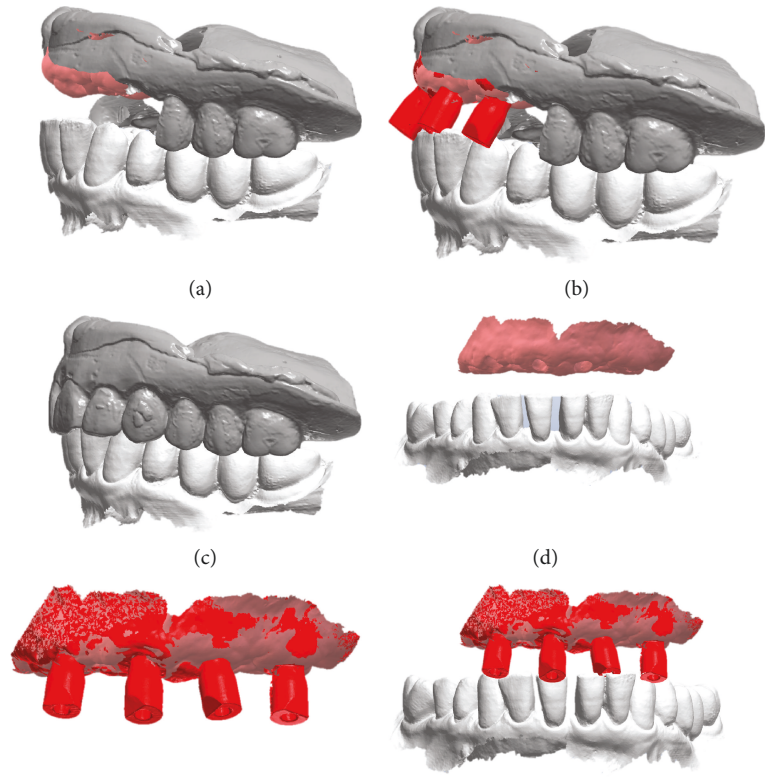

(a) (b)

(c) (d)

(e) (f)

Figure 4: Intraoral scanning with CS 3600® (Carestream Dental, Atlanta, GE, USA), .STL files. The intraoral scan is performed with the patient wearing the copy of the preexisting denture, printed in 3D, properly discarded and opened in the scanbody area. The presence of this copy is essential to give the correct references for the vertical dimension of occlusion. (a) Master model with mucosal collars, antagonist, and copy of the preexisting denture opened in the anterior area; (b) master model with mucosal collars, antagonist, copy of the preexisting denture opened in the anterior area, and scanbodies; (c) copy of the preexisting denture and antagonist arch; (d) master model with mucosal collars and antagonist in the correct spatial relationship; (e) master model with mucous collars and scanbodies; (f) master model with mucosal collars, scanbodies, and antagonist in the correct spatial relationship.

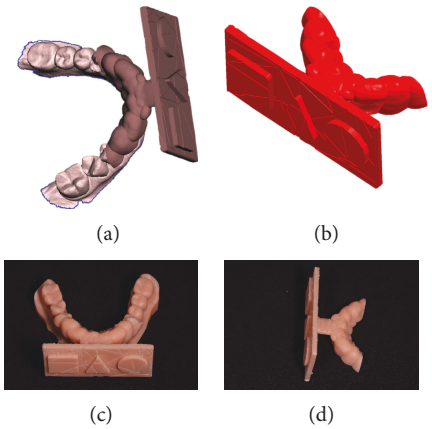

Figure 5: Designing and 3D printing of the individual reference tray (IRT), useful for the superimposition between intraoral scans and face scans. (a) IRT in Meshmixer® and its spatial relationship with the antagonist model; (b) detail of the IRT with known geometry; (c) printing of the tray and the model of the antagonist assembled together; (d) detail of the individual reference tray (IRT).

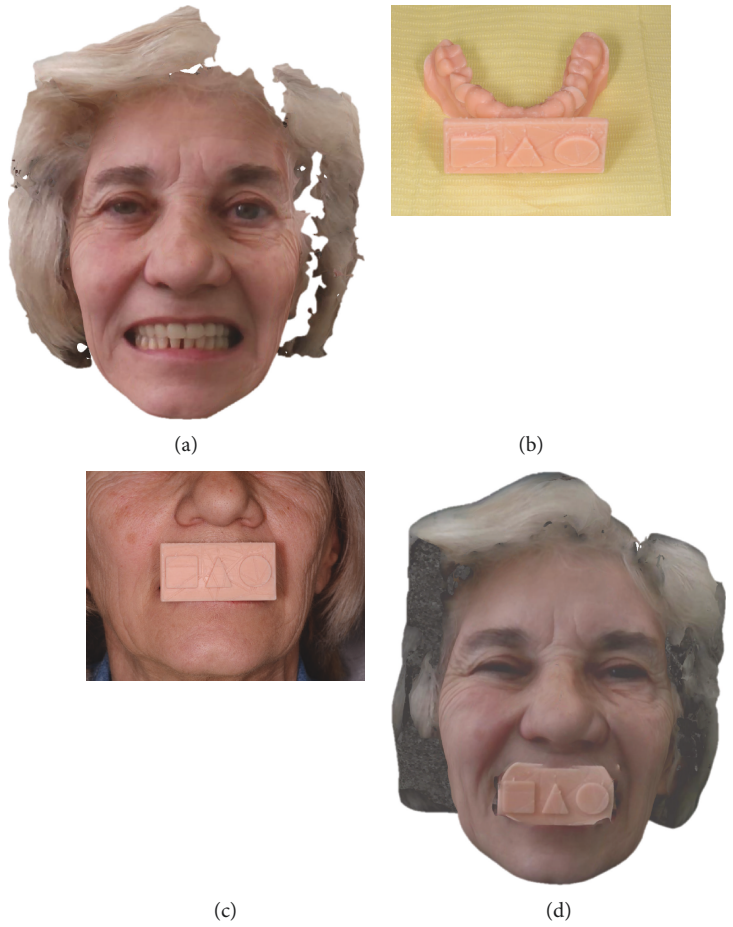

Figure 6: Face scan with OBI® (Fifthingenium, Milan, Italy), performed with the patient wearing a preexisting denture. (a) Face scan without an individual reference tray (IRT); (b) the individual reference tray is ready to be used; (c) extraoral detail of the individual reference tray (IRT) worn by the patient; (d) face scan with OBI® and individual reference tray (IRT).

2.3.3. One-Year Success Rate of the Implant-Supported Overdenture. In the absence of any biologic and prosthetic complications throughout the follow-up period, the implant-supported overdenture was considered successful. Biologic complications would include soft tissue inflammation (peri-implant mucositis) and peri-implant infection (peri-implantitis) with fistula formation, pain, and exudation/suppuration. The threshold for peri-implantitis was set by a probing pocket depth ≥ 6 mm with bleeding on probing and/or pus secretion. Prosthetic complications would

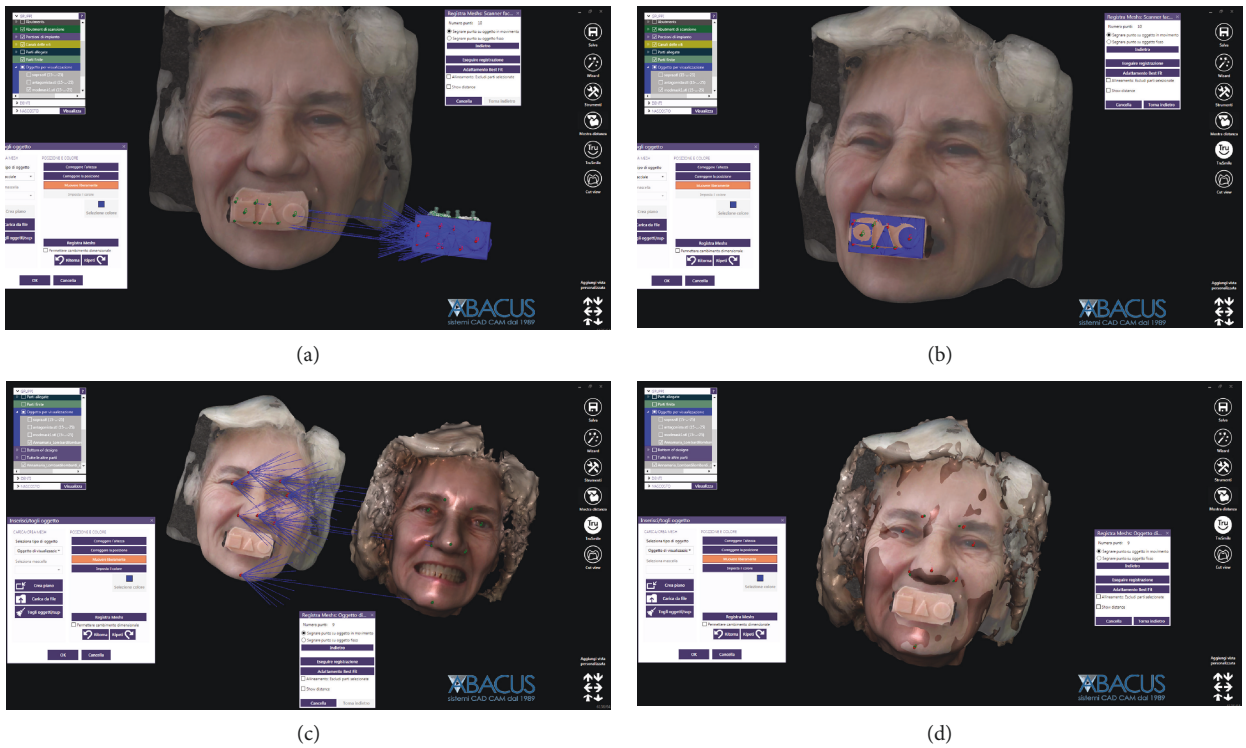

(a) (b) (c) (d)

Figure 7: Import of all files from intraoral scan and face scan into the CAD software (Exocad®), in order to design the bar. (a) Import of face scan with individual reference tray (IRT); (b) superimposition by points and by surfaces of the face scan with individual reference tray (IRT) on the intraoral scan files, using the original CAD drawing of the tray; (c) import of the face scan without individual reference tray (IRT) and its superposition, by points and by surfaces, on the previous face scan, using facial landmarks; (d) when the superimposition is completed, it is now possible to design the bar having the morphology of the patient's face in the correct spatial position, without individual reference tray (IRT).

encompass mechanical problems (loosening of the bar) and technical issues related to anchorage structure (broken bars or loose, lost, or broken attachments) or prostheses (repairs of fractured prostheses or overdenture teeth). The success rate of the overdenture was calculated at the patient level.

2.4. Statistical Evaluation. All data was collected from the records of the patients consecutively enrolled in the study. Descriptive statistics were performed for the patients' demographics (gender, age at start of the prosthetic treatment) and the diameter/length of the implants. Absolute and relative (%) distributions were calculated for qualitative variables (adaptation and passive fit, survival, and success rates). Finally, means, standard deviations, medians, and 95% confidence interval (95% CI) were estimated for quantitative variables (patient's age at start of the prosthetic treatment).

3. Results

The present clinical study was based on a sample of 15 patients (6 males, 9 females, mean age 68.8 ± 4.7 years, range 58–76, median 69, 95% CI: 66.5–71.1) rehabilitated with an implant-retained bar-supported maxillary overdenture. In all patients, the bar was fabricated in PEEK by means of a CAD/CAM procedure and was supported by 4 implants; thus, a total of 60 implants were placed. The distribution of the implants was as reported in Table 1.

At the time of testing the 3D-printed resin bar, 12 bars out of 15 (12/15: 80%) had a perfect passive adaptation and fit and were consequently considered acceptable; the technician could then proceed to mill the definitive PEEK bars. In contrast, 3 out of 15 resin bars (3/15: 20%) did not present a sufficient passive fit or adaptation, due to the presence of movements before screwing or difficulty in the screwing itself. In all these cases, it was therefore necessary to repeat the scanning, modeling, and production procedure. The repetition of the procedure allowed us to solve the problems and proceed with the manufacture of the final PEEK bars in a completely digital flow. At the time of the test and the delivery of the PEEK bars, on the contrary, no problem occurred. All the PEEK bars fit and screwed perfectly with an ideal passive fit and could therefore be safely delivered to the patient.

No implants were lost, for a 1-year implant survival rate of 100% (60/60 surviving implants) (Figure 12).

Conversely, some complications (two fixtures with peri-implantitis, in the same patient; and two repaired overdentures because of tooth fracture, in two different patients) occurred during the follow-up period. This determined a 1-year success rate of 80% (12/15 patients without any complications encountered during the entire follow-up).

4. Discussion

The use of IOS for capturing optical impressions on natural teeth and on implants is rapidly spreading in dental offices

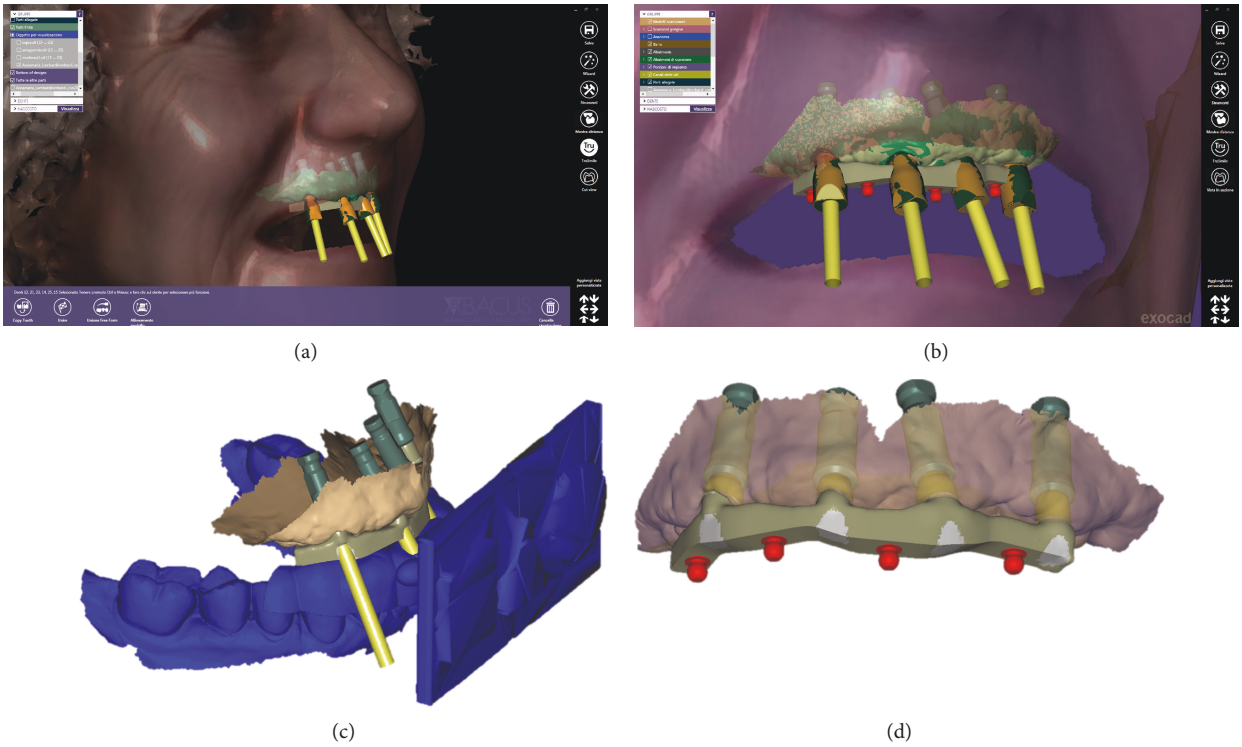

(a) (b)

(c) (d)

Figure 8: Design of the bar with the face references. (a) Detail of the modeled bar and scanbodies; (b) the bar modeled with precision attachments; (c) all the files are perfectly aligned within the CAD; (d) files of the final modeling of the bar.

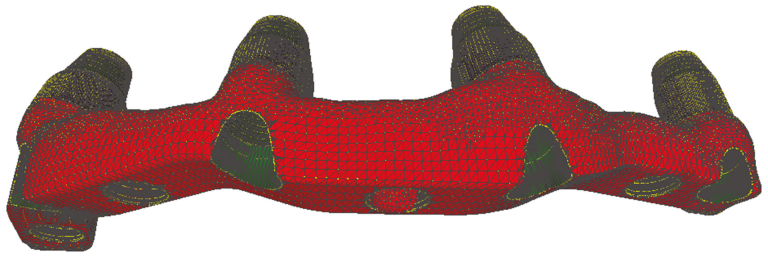

Figure 9: The design of the bar is ready for prototyping.

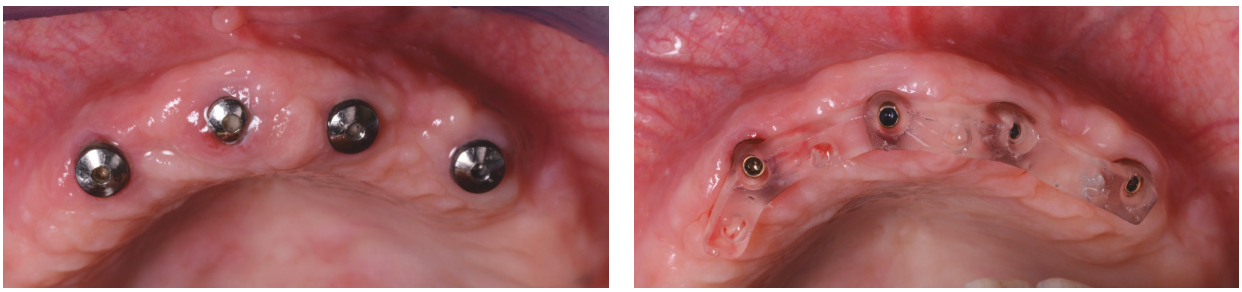

(a) (b)

Figure 10: Test of the passive fit of the 3D-printed bar. (a) Healing abutments before removal; (b) the test of the 3D-printed bar in hard and transparent resin; it is essential to obtain a perfect fit on the implants and a passive fit.

around the world. The process of taking optical impressions is now comfortable for the patient [2, 20, 21] and capturing them is now easy for the clinician; at the same time, IOSs are accurate, as demonstrated by several *in vitro* studies [2, 3, 35], and allow the modeling of simple to complex fixed restorations that have a minimal marginal gap, as shown by several clinical studies [11–13, 16–19].

To date, the literature has not yet clarified whether optical impressions are able to capture quality impressions in the completely edentulous patient, both for fixed

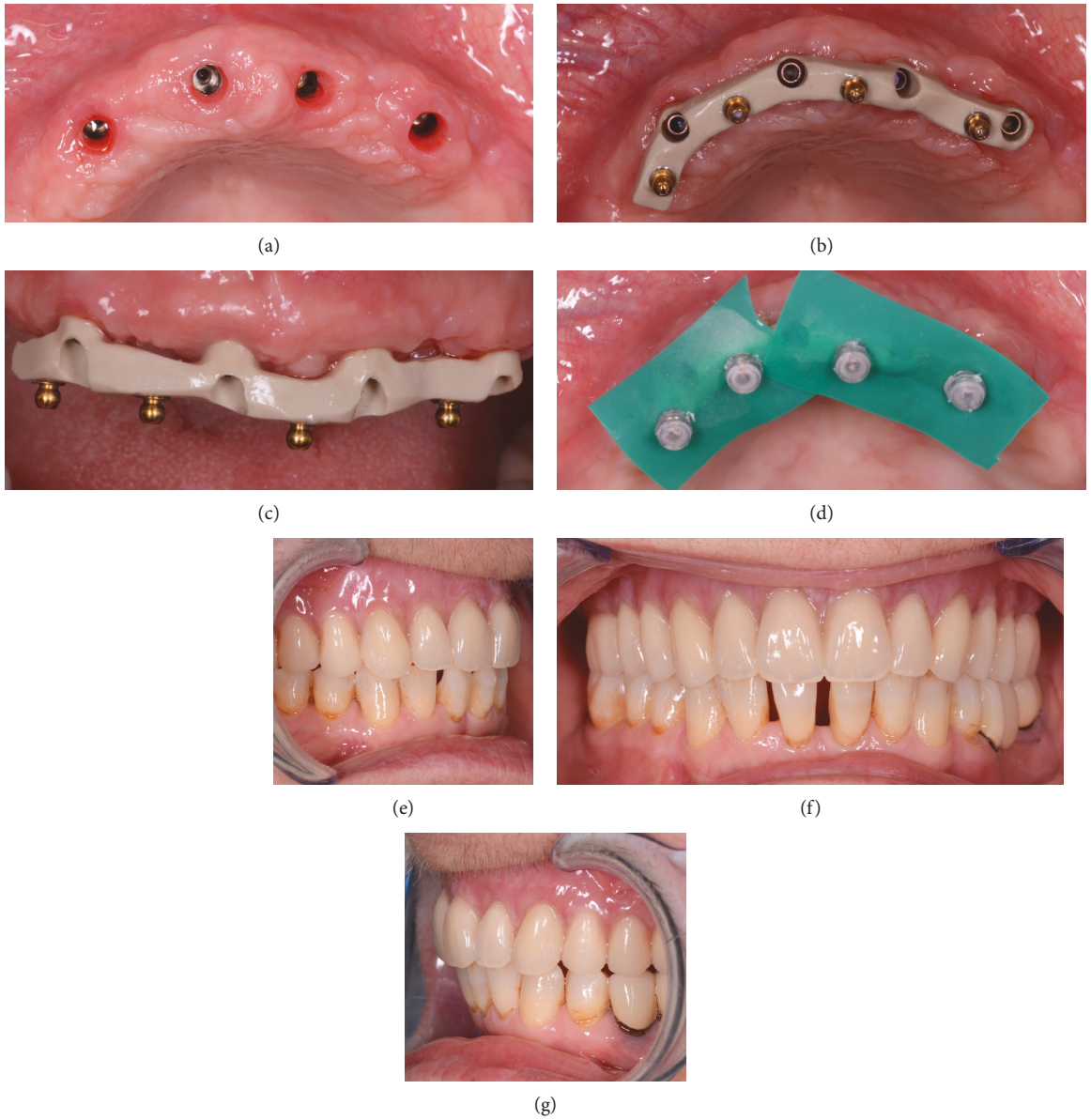

Figure 11: Delivery of the bar and the final overdenture. (a) Removal of healing abutments; (b) definitive PEEK bar, occlusal view; (c) definitive PEEK bar, front view; (d) activation of the prosthesis ball attachments directly in the mouth; (e) definitive overdenture, right side; (f) definitive overdenture, frontal view; (g) definitive overdenture, left side.

Table 1: Distribution of the implants (BTSafe®, BTK, Dueville, Vicenza, Italy) by length and diameter (in mm).

	8 mm	10 mm	12 mm	14 mm	Total
3.3 mm	7	8	5	2	22
3.75 mm	4	6	4	3	17
4.1 mm	5	4	6	1	16
4.8 mm	2	2	1	0	5
Total	18	20	16	6	60

rehabilitations on implants and for the manufacture of removable implant-supported overdentures [22–26].

Despite this, the impressive technological evolution and the improvements in the acquisition software for IOS, with consequent enhancement of accuracy, open up new vistas and make it possible to extend the clinical applications of these instruments today, even to the completely edentulous patient.

In a recent clinical study, Capparè et al. [36] compared the accuracy of digital versus conventional impressions in the totally edentulous maxilla. In all, 50 patients who needed to be rehabilitated with full-arch Toronto screw-retained prostheses, each supported by 6 implants, were allocated to one of two groups: the *test* group (optical impressions with IOS) and the *control* group (conventional impressions) [36]. In the patients of the *test* group, the definitive metal structure of the prosthesis was milled in CAD/CAM, while in the patients of the *control* group, it was carried out in a conventional way [36]. In both groups, the passive fit and

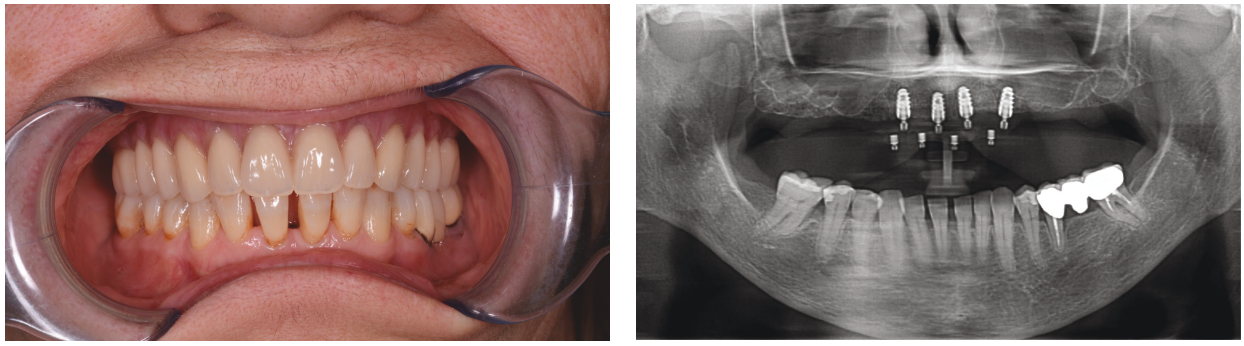

(a) (b)

Figure 12: Clinical and radiographic control at 1 year from implant placement. (a) Frontal clinical photo; (b) panoramic radiograph.

the marginal adaptation of the definitive structure were optimal, as also confirmed radiographically by the analysis of all 300 implants inserted; however, the digital procedure saved a great deal of time in the fabrication of the prosthetic structure [36]. The authors concluded that IOS represents a valid alternative for capturing suitable impressions for the modeling and fabrication of milled bars or structures, in support of full-arch prostheses in the maxilla [36].

This work has the merit of having highlighted how IOS is reliable and accurate in capturing the impression in the completely edentulous maxilla, confirming, in a larger sample of patients, the evidence that emerged in a previous work by the same authors [30]. It should be noted that all the scans were in the maxilla edentula, which is simpler than the edentulous mandible; furthermore, in this study, the implant scanbodies were splinted with resin [36].

Tallarico et al. [37] presented a protocol for the fabrication of overdentures, based on the extraoral chairside digitalization of scan abutments fixed on a specially designed customized tray, based on the original virtual planning. This custom tray allows one to reduce the error involved in intraoral scanning, providing landmarks to the scanner, and thus represents a valid alternative to splinting with resin; moreover, it allows the acquisition of information related to the occlusion register and the vertical dimension of occlusion, which are fundamental not only for the design of the bar but also for the design of the entire prosthesis in CAD/-CAM [37]. In this sense, the use of face scanning can certainly help, in order to provide the technician with the information necessary for modeling, based on the information on the patient's face [37]. The construction of the overdenture in CAD/CAM, as well as that of the complete denture, starting with intraoral scanning, is essentially burdened by two practical problems: (a) the need to capture the scans of the arches in the correct vertical dimension of occlusion and thus in the proper spatial relationships and (b) the need (especially with the conventional removable denture) to obtain impressions that are correctly functionalized [38, 39]. Functionalization means the ability to record all the details of muscle insertions and frenula also in activity, which has always been a key in the making of a complete denture [38, 39]. As one might guess, it is very difficult if not impossible to capture optical impressions with IOS that are functionalized; the IOS, by definition, cannot capture dynamic changes in the soft tissues [38]. Precisely for this reason, the authors of previous studies on the fabrication of full digital removable dentures have always introduced analogic passages within the workflow, precisely because of the need to functionalize [38].

In the present prospective clinical study, 15 patients were enrolled and were rehabilitated with a maxillary bar-retained overdenture. The choice of an overdenture-type restoration (rather than a fixed restoration without fake gingiva) depended in this work on the absence of adequate facial support, as well as on economic (reduced cost) and hygienic reasons (ease of maintaining oral hygiene domiciliary, compared to Toronto fixed and screwed on the implants). The merit of this work was to present a technique for CAD/-CAM fabrication of implant-supported bars for overdentures, starting with intraoral scanning. In this study, most of the CAD/CAM bars (80%) had an excellent passive fit and adaptation, with only a limited number of bars (3/15: 20%), which presented problems of fit and adaptation during the resin test. Although this percentage is rather high, representing about one bar out of five, it must be said that the repetition of the intraoral scan and the new design made it possible to overcome the problems and thus to create new test bars, which fitted perfectly on the implants. The passage through a test bar, 3D printed in resin, seems in this sense essential, before being able to pass to the production of the definitive PEEK bar, which obviously presents higher costs. Note that in all three cases of inadequate adaptation, the distal implants were rather tilted and disparallel to each other. These results seem to confirm the evidence emerged from the most recent studies, which show how the evolution of the software of IOS allows us today to capture sufficiently accurate impressions to support the fabrication of full-arch-type fixed prostheses [30, 31, 36, 37], with at least 4–6 implants. Of course, the accuracy of intraoral scanning depends on many factors, including the scanner used (different scanners give significantly different results) [35], the scanning strategy [40], and the operator's experience. The intraoral scanning strategy is certainly relevant, as different paths can determine different results [40]. In the present study, we have used a zig-zag technique, with the tip describing an arc over the surface of the teeth and scanbodies. This

scanning path was selected because it gave excellent results in previous in vitro studies [3, 35]. In this work, the definitive CAD/CAM bars have been milled in PEEK. This choice is perfectly in tune with the metal-free philosophy, which is growing in digital dentistry; however, clinical studies are still needed to assess the performance and reliability of this material over the medium and long term [41]. In fact, although in this study all implants survived for one year, for a 100% survival rate, it should be noted that complications that were recorded during this study (two fixtures with peri-implantitis in the same patient and two repaired overdentures because of tooth fracture in two different patients) determined a success rate for the implant-prosthetic rehabilitation with overdenture of 80%, at 1 year. These complications must be taken into account, and the behaviour of soft tissues in relation to the PEEK of the bar should be further investigated.

This study has limitations: the low number of patients enrolled in the study, the limited follow-up, and the fact that only the bars (and not the prostheses) were manufactured in CAD/CAM. The limited follow-up is a particularly significant limitation of the present study, since we have used a relatively new material (PEEK) for the manufacture of the bars, which are normally made in metal. There are no long-term studies on the performance of PEEK bars and certainly an evaluation of at least 5 years is required, in order to draw adequate conclusions on the reliability of this method. Moreover, in this study, only the bars were CAD/CAM. The next step is undoubtedly represented by the possibility of using intraoral scans for the design and production of the overdenture prostheses themselves (and not just of the bars). This is technically possible today, using the setting and the acquisition protocol used in the present clinical study. The possibility of using the patient's face scans and working with the files of the prosthetic bases in the correct respective spatial positions, in full compliance with the vertical dimension of occlusion, represents a further merit of this study. The face scan is able to provide information on the patient's face, in 3D, to the dental technician; this information is very useful for modeling not only the bar with the relative dimensions but also and above all the removable overdenture, in full compliance with the tissue volumes [4, 5, 8]. The production of the final prosthesis can then rest on the milling of the pink acrylic prosthetic base and the teeth (which will be glued on top of it), as on 3D printing. Finally, a further limitation of the technique presented in this study is given by the costs of the machines (intraoral and face scanners, 3D printer) and necessary CAD software. The cost of these tools and software is still quite high, and this could limit the spread of the technique, making it not easily accessible to everyone. However, today, many dental practices invest in digital technologies, and it is not even necessary to buy everything: it is possible to rely on one of the many service centers (adequately equipped dental laboratories), at least for CAD software and 3D printers. In any case, when the whole process takes place within the dental clinic, in addition to the investment necessary for the purchase of devices and software, it is also necessary to consider that a learning curve is necessary, in order to learn how to use the machines and software. Digital processes are not simple, and this may represent a further limitation of the present study.

5. Conclusion

In the present clinical study, the integration of intraoral and face scans allowed us to successfully restore 15 fully edentulous maxillae maxillary overdentures supported by 4 implants and a CAD/CAM polyether-ether-ketone (PEEK) bar. In fact, when testing the 3D-printed resin bars (replicas), 12 bars out of 15 (12/15: 80%) had a perfect passive adaptation and fit and were consequently considered acceptable, i.e., the technician could proceed to mill the definitive PEEK bars. In contrast, three out of 15 bars (3/15: 20%) did not present a sufficient passive fit or adaptation, due to the presence of movements before screwing or difficulty in the screwing itself. In all these cases, it was necessary to repeat the scanning, modeling, and production procedure. The repetition of the procedure, however, allowed to solve the problems and proceed with the manufacture of the final PEEK bars in a completely digital flow. A 100% implant survival rate was found in this study; however, some complications (two fixtures with peri-implantitis in the same patient and two repaired overdentures because of tooth fracture in two different patients) occurred during the follow-up period, for a success rate of 80% for the implant-supported overdenture treatment. The digital procedures have the potential to decrease patient discomfort and to reduce the laboratory work associated with the fabrication of implant-supported overdentures. In addition, the use of PEEK can eliminate the need of using metals for the fabrication of the bar. However, this study has limitations, and further investigation is needed to confirm the outcomes emerging from this research.

Data Availability

Data are available from the corresponding author upon reasonable request.

Disclosure

No funding nor materials were received from third parties.

Conflicts of Interest

The authors report no conflict of interest related to the preparation of the present study.

Acknowledgments

This study was self-funded.

References

[1] F. Mangano, J. A. Shibli, and T. Fortin, "Digital dentistry: new materials and techniques," *International Journal of Dentistry*, vol. 2016, Article ID 5261247, 2 pages, 2016.

[2] F. Mangano, A. Gandolfi, G. Luongo, and S. Logozzo, "Intraoral scanners in dentistry: a review of the current literature," *BMC Oral Health*, vol. 17, no. 1, p. 149, 2017.

[3] M. Imburgia, S. Logozzo, U. Hauschild, G. Veronesi, C. Mangano, and F. G. Mangano, "Accuracy of four intraoral scanners in oral implantology: a comparative in vitro study," *BMC Oral Health*, vol. 17, no. 1, p. 92, 2017.

[4] B. Hassan, M. Greven, and D. Wismeijer, "Integrating 3D facial scanning in a digital workflow to CAD/CAM design and fabricate complete dentures for immediate total mouth rehabilitation," *The Journal of Advanced Prosthodontics*, vol. 9, no. 5, pp. 381–386, 2017.

[5] B. Hassan, B. Gimenez Gonzalez, A. Tahmaseb, M. Greven, and D. Wismeijer, "A digital approach integrating facial scanning in a CAD-CAM workflow for complete-mouth implant-supported rehabilitation of patients with edentulism: a pilot clinical study," *Journal of Prosthetic Dentistry*, vol. 117, no. 4, pp. 486–492, 2017.

[6] R. Jacobs, B. Salmon, M. Codari, B. Hassan, and M. M. Bornstein, "Cone beam computed tomography in implant dentistry: recommendations for clinical use," *BMC Oral Health*, vol. 18, no. 1, p. 88, 2018.

[7] C. Mangano, F. Luongo, M. Migliario, C. Mortellaro, and F. G. Mangano, "Combining intraoral scans, cone beam computed tomography and face scans: the virtual patient," *Journal of Craniofacial Surgery*, vol. 29, no. 8, pp. 2241–2246, 2018.

[8] T. Joda, U. Bragger, and G. Gallucci, "Systematic literature review of digital three-dimensional superimposition techniques to create virtual dental patients," *The International Journal of Oral & Maxillofacial Implants*, vol. 30, no. 2, pp. 330–337, 2015.

[9] T. Joda, W. Derksen, J. G. Wittneben, and S. Kuehl, "Static computer-aided implant surgery (s-CAIS) analysing patient-reported outcome measures (PROMs), economics and surgical complications: a systematic review," *Clinical Oral Implants Research*, vol. 29, supplement 16, pp. 359–373, 2018.

[10] F. G. Mangano, U. Hauschild, and O. Admakin, "Full in-office guided surgery with open selective tooth-supported templates: a prospective clinical study on 20 patients," *International Journal of Environmental Research and Public Health*, vol. 15, no. 11, p. 2361, 2018.

[11] T. Joda, M. Ferrari, G. O. Gallucci, J. G. Wittneben, and U. Bragger, "Digital technology in fixed implant prosthodontics," *Periodontology 2000*, vol. 73, no. 1, pp. 178–192, 2017.

[12] M. B. Blatz and J. Conejo, "The current state of chairside digital dentistry and materials," *Dental Clinics of North America*, vol. 63, no. 2, pp. 175–197, 2019.

[13] T. Joda, F. Zarone, and M. Ferrari, "The complete digital workflow in fixed prosthodontics: a systematic review," *BMC Oral Health*, vol. 17, no. 1, p. 124, 2017.

[14] G. Lecocq, "Digital impression-taking: fundamentals and benefits in orthodontics," *International Orthodontics*, vol. 14, no. 2, pp. 184–194, 2016.

[15] R. van Noort, "The future of dental devices is digital," *Dental Materials*, vol. 28, no. 1, pp. 3–12, 2012.

[16] R. Eftekhar Ashtiani, L. Nasiri Khanlar, M. Mahshid, and A. Moshaverinia, "Comparison of dimensional accuracy of conventionally and digitally manufactured intracoronal restorations," *Journal of Prosthetic Dentistry*, vol. 119, no. 2, pp. 233–238, 2018.

[17] T. Joda, U. Bragger, and N. U. Zitzmann, "CAD/CAM implant crowns in a digital workflow: five-year follow-up of a prospective clinical trial," *Clinical Implant Dentistry and Related Research*, vol. 21, no. 1, pp. 169–174, 2019.

[18] F. Mangano, B. Margiani, and O. Admakin, "A novel full-digital protocol (SCAN-PLAN-MAKE-DONE®) for the design and fabrication of implant-supported monolithic translucent zirconia crowns cemented on customized hybrid abutments: a retrospective clinical study on 25 patients," *International Journal of Environmental Research and Public Health*, vol. 16, no. 3, p. 317, 2019.

[19] G. I. Benic, I. Sailer, M. Zeltner, J. N. Gutermann, M. Ozcan, and S. Muhlemann, "Randomized controlled clinical trial of digital and conventional workflows for the fabrication of zirconia-ceramic fixed partial dentures. Part III: marginal and internal fit," *Journal of Prosthetic Dentistry*, vol. 121, no. 3, pp. 426–431, 2019.

[20] A. Mangano, M. Beretta, G. Luongo, C. Mangano, and F. Mangano, "Conventional vs digital impressions: acceptability, treatment comfort and stress among young orthodontic patients," *The Open Dentistry Journal*, vol. 12, no. 1, pp. 118–124, 2018.

[21] E. Yuzbasioglu, H. Kurt, R. Turunc, and H. Bilir, "Comparison of digital and conventional impression techniques: evaluation of patients' perception, treatment comfort, effectiveness and clinical outcomes," *BMC Oral Health*, vol. 14, no. 1, p. 10, 2014.

[22] P. Ahlholm, K. Sipila, P. Vallittu, M. Jakonen, and U. Kotiranta, "Digital versus conventional impressions in fixed prosthodontics: a review," *Journal of Prosthodontics*, vol. 27, no. 1, pp. 35–41, 2018.

[23] A. Di Fiore, R. Meneghello, L. Graiff et al., "Full arch digital scanning systems performances for implant-supported fixed dental prostheses: a comparative study of 8 intraoral scanners," *Journal of Prosthodontic Research*, 2019.

[24] S. Muhlemann, R. D. Kraus, C. H. F. Hammerle, and D. S. Thoma, "Is the use of digital technologies for the fabrication of implant-supported reconstructions more efficient and/or more effective than conventional techniques: a systematic review," *Clinical Oral Implants Research*, vol. 29, supplement 18, pp. 184–195, 2018.

[25] M. Y. Tan, S. H. X. Yee, K. M. Wong, Y. H. Tan, and K. B. C. Tan, "Comparison of three-dimensional accuracy of digital and conventional implant impressions: effect of interimplant distance in an edentulous arch," *The International Journal of Oral & Maxillofacial Implants*, vol. 34, no. 2, pp. 366–380, 2019.

[26] A. Ender, M. Zimmermann, and A. Mehl, "Accuracy of complete- and partial-arch impressions of actual intraoral scanning systems *in vitro*," *International Journal of Computerized Dentistry*, vol. 22, no. 1, pp. 11–19, 2019.

[27] G. Heydecke, M. Zwahlen, A. Nicol et al., "What is the optimal number of implants for fixed reconstructions: a systematic review," *Clinical Oral Implants Research*, vol. 23, Supplement 6, pp. 217–228, 2012.

[28] T. Spielau, U. Hauschild, and J. Katsoulis, "Computer-assisted, template-guided immediate implant placement and loading in the mandible: a case report," *BMC Oral Health*, vol. 19, no. 1, p. 55, 2019.

[29] C. Mangano, F. Mangano, J. A. Shibli, M. Ricci, R. L. Sammons, and M. Figliuzzi, "Morse taper connection implants supporting "planned" maxillary and mandibular bar-retained

overdentures: a 5-year prospective multicenter study," *Clinical Oral Implants Research*, vol. 22, no. 10, pp. 1117–1124, 2011.

[30] E. Gherlone, P. Capparè, R. Vinci, F. Ferrini, G. Gastaldi, and R. Crespi, "Conventional versus digital impressions for "all-on-four" restorations," *The International Journal of Oral & Maxillofacial Implants*, vol. 31, no. 2, pp. 324–330, 2016.

[31] M. Tallarico, D. Schiappa, F. Schipani, F. Cocchi, M. Annucci, and E. Xhanari, "Improved fully digital workflow to rehabilitate edentulous patient with an implant overdenture in 4 appointments: a case report," *Journal of Oral Science and Rehabilitation*, vol. 3, no. 3, pp. 38–46, 2017.

[32] H. Chen, N. Liu, X. Xu, X. Qu, and E. Lu, "Smoking, radiotherapy, diabetes and osteoporosis as risk factors for dental implant failure: a meta-analysis," *PLoS One*, vol. 8, no. 8, article e71955, 2013.

[33] G. A. Dolcini, M. Colombo, and C. Mangano, "From guided surgery to final prosthesis with a fully digital procedure: a prospective clinical study on 15 partially edentulous patients," *International Journal of Dentistry*, vol. 2016, Article ID 7358423, 7 pages, 2016.

[34] F. G. Mangano, J. T. Pires, J. A. Shibli et al., "Early bone response to dual acid-etched and machined dental implants placed in the posterior maxilla: a histologic and histomorphometric human study," *Implant Dentistry*, vol. 26, no. 1, pp. 24–29, 2017.

[35] F. G. Mangano, U. Hauschild, G. Veronesi, M. Imburgia, C. Mangano, and O. Admakin, "Trueness and precision of 5 intraoral scanners in the impressions of single and multiple implants: a comparative in vitro study," *BMC Oral Health*, vol. 19, no. 1, p. 101, 2019.

[36] P. Capparè, G. Sannino, M. Minoli, P. Montemezzi, and F. Ferrini, "Conventional versus digital impressions for full arch screw-retained maxillary rehabilitations: a randomized clinical trial," *International Journal of Environmental Research and Public Health*, vol. 16, no. 5, p. 829, 2019.

[37] M. Tallarico, E. Xhanari, M. Martinolli, E. Baldoni, and S. M. Meloni, "Extraoral chairside digitalization: clinical reports on a new digital protocol for surgical and prosthetic treatment of completely edentulous patients," *Journal of Oral Science and Rehabilitation*, vol. 4, no. 2, pp. 16–20, 2018.

[38] A. Unkovskiy, E. Wahl, A. T. Zander, F. Huettig, and S. Spintzyk, "Intraoral scanning to fabricate complete dentures with functional borders: a proof-of-concept case report," *BMC Oral Health*, vol. 19, no. 1, p. 46, 2019.

[39] G. Bonnet, C. Batisse, M. Bessadet, E. Nicolas, and J. L. Veyrune, "A new digital denture procedure: a first practitioners appraisal," *BMC Oral Health*, vol. 17, no. 1, p. 155, 2017.

[40] P. Medina-Sotomayor, M. Agustín Pascual, and A. Isabel Camps, "Accuracy of four digital scanners according to scanning strategy in complete-arch impressions," *PLoS One*, vol. 13, no. 9, article e0202916, 2018.

[41] O. A. L. Jaros, G. A. P. De Carvalho, A. B. G. Franco, S. Kreve, P. A. B. Lopes, and S. C. Dias, "Biomechanical behavior of an implant system using polyether ether ketone bar: finite element analysis," *Journal of International Society of Preventive & Community Dentistry*, vol. 8, no. 5, pp. 446–450, 2018.